ChemElectroChem
Minireviews
doi.org/10.1002/celc.202100484
Chemistry Europe
European Chemical Societies Publishing

Advancing Electrolyte Solution Chemistry and Interfacial Electrochemistry of Divalent Metal Batteries

Hui Wang,[a, f] Jaegeon Ryu,[a, f] Yuyan Shao,*[a, f] Vijayakumar Murugesan,[b, f] Kristin Persson,[c, d, f] Kevin Zavadil,[e, f] Karl T. Mueller,[b, f] and Jun Liu[a]

Divalent metal (Mg, Ca, etc.) battery chemistries potentially provide a sustainable long-term technical solution for large-scale energy storage because of the high natural abundance of divalent metal elements in the earth crust. Good progress has been made on materials especially electrolyte development in the past years; however, significant challenges exist, particularly the very limited fundamental understanding of electrolyte solution chemistry and interfacial electrochemistry. In this perspective, we review and discuss key discoveries and understanding of divalent battery chemistry with a focus on electrolyte-dependent interfacial electrochemistry of divalent metal anodes. A concise review of electrolyte development, operando studies of the electrified interfaces, and unique charge-transfer process is provided; the knowledge gaps and future research directions are discussed.

1. Introduction

Divalent metal electrochemistry and interfacial chemistry is the foundation of divalent metal battery technology development. In the past years, there has been good progress in materials discovery for divalent batteries;[1] however, limited fundamental understanding of divalent interfacial electrochemistry indicates this is still an under-explored field, which presents great opportunities for scientific discoveries that may lead to disruptive battery technology development. Battery energy storage is playing an ever-increasing, important role in today's society, driven by the electrification of transportation, smart grid, portable devices, and other applications. While the state-of-the-art battery technology, Li-ion battery (LIB), has enabled portable electrical devices broadly and is transforming the electric transportation and reliable renewable grid, there are potentially some concerns about its cost, safety, and resource limitation. Divalent metals (*e.g.* Mg, Ca, etc.) provide great potential to address these concerns. Divalent battery chemistry, such as Mg^{2+} and Ca^{2+}, can offer significant improvements in the volumetric capacity (Mg: 3833 $mAh\,cm^{-3}$; Ca: 2073 $mAh\,cm^{-3}$ vs. Li: 2062 $mAh\,cm^{-3}$); The divalent metals are much more abundant in the earth crust (Mg: 23300 ppm, Ca: 41500 ppm vs. Li: 20 ppm), thus drastically reducing the cost and environmental impact of producing raw materials (Mg: \$ 0.26 g^{-1}, Ca: \$ 0.66 g^{-1} vs. Li: \$ 1.44 g^{-1}).[2]

Although divalent batteries can potentially achieve high volumetric energy densities using metallic anodes, discovering a single electrolyte, which is capable of reversible divalent metal *plating/stripping* at the anode and supporting reversible intercalation/deintercalation in high-voltage cathodes, remains a significant scientific and technical challenge.[2b,c, 3] Especially, the high charge density of M^{2+} (Mg^{2+}: 120 $C\,mm^{-3}$, Ca^{2+}: 52 $C\,mm^{-3}$ vs. Li^{+}: 52 $C\,mm^{-3}$) poses a huge energy barrier for solid-state diffusion of divalent ions in the bulk host materials and within the interfacial layer on the surface.[2c] The development of versatile divalent electrolytes has been curbed by multiple factors such as limited chemical and electrochemical compatibility with the electrodes (*i.e.* narrow electrochemical stability window),[2b] lack of reversible divalent metal *plating/stripping*, instability against current collectors, low divalent ion mobility, the formation of ion pairs (*i.e.* low divalent cation transference number: t^{+}) and low Coulombic efficiency (CE).

Among them, reversible electrochemical *plating/stripping* of divalent metals is a limiting step for developing rechargeable divalent metal batteries, in which electrolytes play an essential role. The interphase chemistry has been well-studied in the alkali metal (*e.g.* Li, Na, K, etc) batteries, where a solid electrolyte interphase (SEI) can permit the monovalent cations to migrate and facilitate the charge-transfer process during *plating/stripping.* However, it is still debatable whether the SEI model applies to the divalent metal anodes due to different chemical reactivity and higher cation charge density. Roles of

---

[a] *Dr. H. Wang, Dr. J. Ryu, Dr. Y. Shao, Dr. J. Liu*
Energy & Environment Directorate
Pacific Northwest National Laboratory
Richland, Washington, 99352, United States
E-mail: yuyan.shao@pnnl.gov
[b] *Dr. V. Murugesan, Dr. K. T. Mueller*
Physical and Computational Sciences Directorate
Pacific Northwest National Laboratory
Richland, Washington, 99352, United States
[c] *Prof. Dr. K. Persson*
Energy Technologies Area
Lawrence Berkeley National Laboratory
Berkeley, California 94720, United States
[d] *Prof. Dr. K. Persson*
Department of Materials Science and Engineering
University of California, Berkeley
Berkeley, California 94720, United States
[e] *Dr. K. Zavadil*
Material, Physical, and Chemical Sciences
Sandia National Laboratories
Albuquerque, New Mexico 87185, United States
[f] *Dr. H. Wang, Dr. J. Ryu, Dr. Y. Shao, Dr. V. Murugesan, Prof. Dr. K. Persson, Dr. K. Zavadil, Dr. K. T. Mueller*
Joint Center for Energy Storage Research (JCESR)
Lemont, Illinois 60439, United States

the electrified interface between electrolytes and divalent metal anodes are yet to be fully elucidated for reversible *plating/stripping*, which is the main topic of this review. Different from previous critical reviews on anodes (including alloys),[4] electrolytes,[2b,3a,b,5] cathode materials,[2c,6] overall system progress,[7] in this paper, we mainly focus on advances of the interface chemistry on divalent metal anodes in terms of cation solvation and coordination, interfacial charge-transfer, and dynamic surface layer (Figure 1). Before we discuss interface chemistry, we need to understand electrolyte systems including solution coordination chemistry for divalent metal batteries.

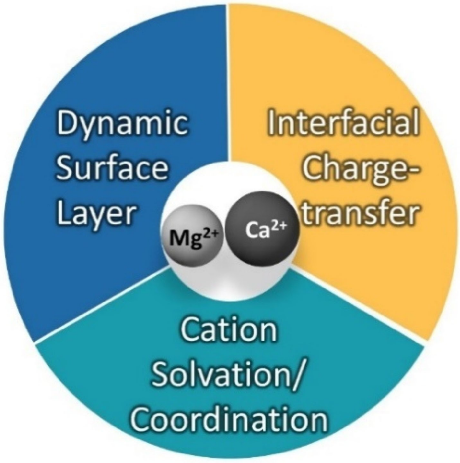

Figure 1. Parameters dictating the interphase chemistry on divalent metal anodes.

2. Electrolytes and Electrolyte-dependent Interfaces

2.1. Electrolyte Design and Development

2.1.1. Grignard-based Electrolytes

The first successful demonstration of Mg *plating/stripping* can date back to the early 20th century in Grignard reagents (**RMgX**, where R is an alkyl or aryl group, and X is Cl or Br) in ethereal solutions,[8] in which Mg electrodeposits are not passivated. However, they are not suitable electrolytes for real applications due to their intrinsically reducing power and poor oxidative (i.e. anodic) stability (typically less than 1.5 V vs. $Mg^{0}/^{2+}$ on Pt working electrode (WE)). The pioneering work by Gregory *et al.* in 1990[9] suggested that the addition of strong Lewis acids (*e.g.* $AlCl_3$ and organoborates[10]-$BBu_2Ph_2^-$, *etc.*) into Grignard reagents can improve the anodic stability, and this strategy was later further developed into the **DCC** ("Dichloro Complex") electrolyte family, which is based on the reaction products of the Lewis bases R_xMgCl_{2-x} with a variety of Lewis acids R'_yAlCl_{3-y} (R, R' = n-butyl and/or ethyl, x = 0–2, y = 0–3) in tetrahydrofuran (**THF**) solutions.[11] The equilibrium electroactive species are the consequence of **transmetalation** reactions, where the organic and inorganic ligands are rapidly exchanged between the Mg and Al cores, and have improved oxidative stability to *ca.* 2.2 V on Pt. Incorporating the electron-withdrawing halogen ligands on the organoaluminate core extended the electrochemical window of the solution without compromising the reversibility of the Mg deposition-dissolution process. Nonetheless, the limited anodic stability of these electrolytes is associated with the relatively weak aluminum-carbon bond that electrochemically breaks via β-H-elimination. The aliphatic ligands were further substituted by phenyl (*i.e.* PhMgCl as the new Lewis base), which does not possess β hydrogen, by Aurbach *et al.* in 2011 to develop the all phenyl complex (**APC**)-type

Dr. Hui Wang was a postdoc (JCESR I/II) in the Battery Materials and Systems group at Pacific Northwest National Laboratory. He received his Ph.D. in Materials Science & Engineering from Mie University (2014), Japan, and then became a battery program researcher under the ALCA-SPRING (JST, Japan). He specializes in the development of electrolytes and electrode materials and the regulation of the interphase chemistry for post/beyond Lithium-ion batteries.

Dr. Jaegeon Ryu is currently a postdoc (JCESR) in the Battery Materials and Systems group at Pacific Northwest National Laboratory. After receiving his Ph.D. in Energy Engineering from the Ulsan National Institute of Science and Technology (UNIST) (2018), he joined the Pohang University of Science and Technology (POSTECH) as a postdoc. He specializes in the development of electrode materials and electrolytes for high-performance rechargeable batteries.

Dr. Yuyan Shao studied Applied Chemistry with a focus on electrochemistry at Harbin Institute of Technology and obtained his B.S. in 2001 and Ph.D. in 2006. He is currently a Chief Scientist and Team Leader at Pacific Northwest National Laboratory. His research interests are focused on fundamental understanding and materials innovation for electrochemical energy storage and conversion.

electrolytes;[12] the resultant new electrolytes push the oxidative stability to *ca.* 3.3 V on Pt.

A boron-based electrolyte,[13] similar to the APC electrolyte, through the reaction of tris(3,5-dimethylphenyl)borane (Mes_3B) and PhMgCl in **THF**, was developed by Yang *et.al.* in 2012. It is now well-accepted that the Lewis base of organomagnesium halide does not exist in ethereal solvents as single compounds, but rather an equilibrium mixture of various compounds (*i.e.* **Schlenk** equilibrium) including high nucleophilic R_2Mg or Ph_2Mg.[9] To expand the cathode material pool limited by these nucleophilic species, the same **transmetalation** route was employed to prepare a non-nucleophilic electrolyte of $[Mg_2(\mu\text{-}Cl)_3\cdot 6\mathbf{THF}][HMDSAlCl_3]$ (**HMDS**: hexamethyldisilazide) that has an electrochemical window up to 3.2 V on Pt,[14] in which **HMDSMgCl** is a non-nucleophilic Lewis base and $AlCl_3$ is the Lewis acid. Other solutions using alkoxides,[15] borates,[16] coupled with $AlCl_3$,[17] have been proposed to prepare electrolytes with favorable characteristics. Later, the inorganic Mg aluminum chloride complex (*i.e.* **MACC**) was further presented which comprises the acid-base reaction products between $MgCl_2$ and $AlCl_3$ in **THF**.[18] One drawback of these electrolytes, based on **transmetalation** strategy, is that they prohibit the exploration of organic anionic supporting ligands and introduce other metals that lead to undesirable side reactions (*i.e.* Al co-deposition). Besides, the inorganic chloride was found to be the only suitable anionic supporting ligand for Mg ions in these systems.[19] However, the presence of halide ions corrodes battery components, which push the community to develop halogen-free Mg salts, which possess high oxidative (anodic) stabilities, high anti-corrosion stability, and high compatibility with Mg metal.

2.1.2. Carborane-based Electrolytes

The monoanionic icosahedral closo-carborane-$\mathbf{HCB_{11}H_{11}}^-$ was discovered by Mohatadi *et al.* in 2015 as an excellent candidate to replace Cl^-,[20] because the anionic charge is part of the cage bonding and fully delocalized over this 12-vertex cage. Further, some substituted $\mathbf{HCB_{11}H_{11}}^-$ anions, lacking lone pairs of electrons and nucleophilic sites, are among the weakest coordinating anions. The new electrolyte formulation of Mg-$(\mathbf{HCB_{11}H_{11}})_2$/tetraglyme (**G4**) possesses a wide electrochemical window of 3.6 V on Pt and 99% CE calculated by the charges passed during Mg *plating/stripping* in cyclic voltammetry (CV) scan (CV method) over 100 cycles. Later, the synthesis of $Mg(\mathbf{HCB_{11}H_{11}})_2$[21] and Mg $(\mathbf{HCB_9H_9})_2$[22] was reported in 2015–2017 through a different cation reduction synthesis methodology. The oxidation of this parent anion of $\mathbf{HCB_{11}H_{11}}^-$ in different solvents was systematically studied with coupled computational and experimental methods in 2018;[23] it was revealed that the anodic stability of the $\mathbf{HCB_{11}H_{11}}^-$ anion is defined by its oxidation to a neutral radical at 4.6 V (on Pt), independent of the solvent employed (Figure 2a). Most recently, the low solubility of $Mg(\mathbf{HCB_{11}H_{11}})_2$ in less coordinating ethers has been improved by the solvent blends such as dimethoxyethane (**DME**)/diglyme (**G2**), **THF**/**DME** or **G2**, DME/dioxolane (**DOL**).[24] A derivatization example of $\mathbf{FCB_{11}H_{11}}^-$ was demonstrated with an even broader electrochemical window of 4.9 V on Pt. The high anodic stability is possibly associated with the passivation layer, which is formed by a rapid reaction between $\mathbf{RCB_{11}H_{11}}^{\cdot}$ radicals in either the H^- or F^- terminated anion with the anion, solvent, or impurities.

Despite the favorable properties of Cl^--free electrolytes, the nontrivial synthesis, and the associated high costs would be a

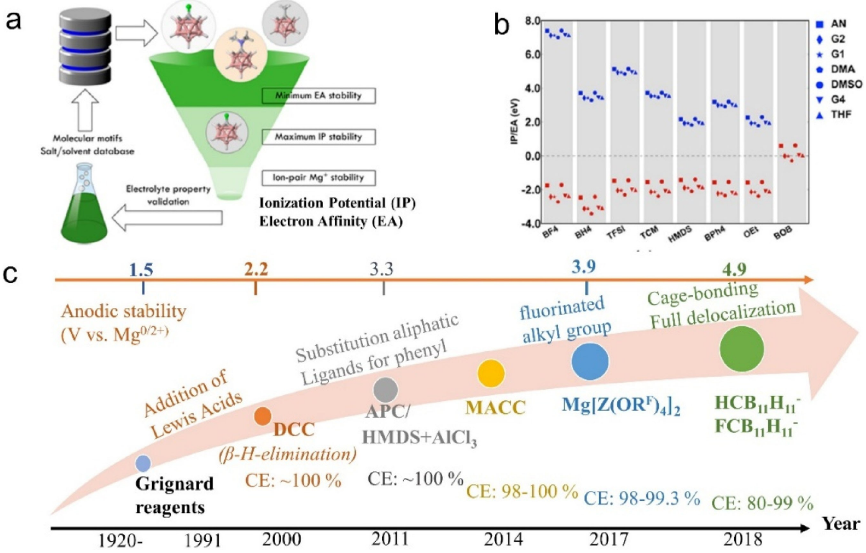

Figure 2. Rational designs of the counter anion in the divalent metal chemistry. a) Coupled computational screening and experimental validation were used to identify electrochemically stable $RCB_{11}H_{11}^-$ anion derivatives. Reproduced with permission from.[23] Copyright 2018 American Chemical Society; b) Calculated electrochemical windows (IP/EA) of different salt anions in different solvent dielectric media. All the values are reported vs. Mg^{2+}/Mg, and the solvent effect is considered by the IEF-PCM model. IP/EA of well-solvated anion where red dots are EAs (electron affinity: the energy gained for a reduced anion); blue dots are IPs (ionization potential: the energy penalty to oxidize an anion). Reproduced with permission from.[31] Copyright 2015 American Chemical Society. c) A brief history of Mg electrolyte breakthroughs with a tradeoff between expanded electrochemical windows and inferior reversibility of Mg *plating/stripping*.

major drawback from the application point of view. It is of importance to develop “simple” electrolytes, *i.e.*, consisting of metal salts with well-defined cation and anion in the common organic solvents such as **THF**, glymes, etc., like those for Li-ion batteries. $Mg(PF_6)_2$, a compound previously considered incapable of reversible Mg deposition, was demonstrated with favorable electrochemical behavior in acetonitrile (**AN**).[25] The only “simple” and commercially available combinations of salt and solvent for reversible Mg electrodeposition, include Mg bis (trifluoromethanesulfonyl)imide ($Mg(TFSI)_2$),[26] Mg trifluoromethanesulfonate (Mg Triflate(OTf)),[27] Mg borohydride ($Mg(BH_4)_2$),[28] and $MgCl_2$.[26b] Despite moderate improvements with these salts dissolved in glyme solvents,[26,29] or ionic liquids,[30] the overall electrolyte performance (electrochemical reversibility of *plating/stripping* and anodic stability) is still far from being practical for battery systems.

2.1.3. Fluorinated Alkoxy-based Electrolytes

New Mg salts are continuously developed with readily resourced materials that can enable high conductivity, reversibility, and compatibility. Inspired by electrolyte designs for Li-ion batteries,[32] the bulky and weakly coordinating anions are of interest due to their expanded electrochemical window. A facile method of synthesizing Mg-tetrakis (hexafluoroisopropyloxy)aluminate (Al(**hfip**)$_4^-$) (Mg[Al(**hfip**)$_4$]$_2$) was reported in 2016[33] and the mixture of this salt in **DME** can impart a near 100% CE calculated by CV method for Mg *plating/stripping* and an enhanced electrochemical window of >3.5 V (vs. Mg^{2+}/Mg on glassy carbon (GC)). Besides, a class of compounds ($Mg[Z(OR^F)_4]_2$, where Z=Al or B; R^F = fluorinated alkyl group) was presented using a more robust, facile, versatile route of the **anion metathesis reaction**.[34] Remarkably, the as-prepared solution of 0.60 M Mg[B(**hfip**)$_4$]$_2$ in **DME** presents anodic stability up to 4.3 V on the stainless steel (SS) and Al, which surpasses that of the **DME** solvent. Compared to alkyloxyaluminate anions, alkyloxyborate anions are lighter and generally less water sensitive. The alkyloxyborate anion of B(**hfip**)$_4^-$ has recently attracted increasing attention. One-step *in situ* reaction of tris(hexafluoroisopropyl)borate [B(**hfip**)$_3$]), $MgCl_2$[35] or MgF_2[36] and Mg powder enabled the preparation of Mg[B(**hfip**)$_4$]$_2$-based electrolytes.[37]

Recently, synthesis of Ca[B(**hfip**)$_4$]$_2$ was realized via a clean and straightforward route by reacting $Ca(BH_4)_2$ with hexafluorisopropanol (**hfip**) in **DME** in 2019.[38] It can be prepared from Ca(**hfip**)$_2$ and B(**hfip**)$_3$ through the Lewis acid-base reaction analogous to the reported Mg[Al(**hfip**)$_4$]$_2$ by Arnold *et al.* in 2019.[39] Despite these advances based on Al(**hfip**)$_4^-$ or B(**hfip**)$_4^-$ anions,[40] their lack of chemical stability under ambient temperature still poses a challenge as they undergo chemical decomposition in the presence of trace moisture. Recently, Liu *et al.* reported a more stable salt of Mg fluorinated pinacolatoborate-$Mg[B(O_2C_2(CF_3)_4)_2]_2$ (Mg-**FPB**), which has strongly coordinating perfluorinated pinacolato bidentate ligands to stabilize the boron center in 2019.[41] The Mg-**FPB**/**G2** solution showed an outstanding electrochemical performance of 95% CE calculated by CV method, low overpotential for reversible Mg deposition, and anodic stability up to 4.0 V on SS, Ti, Al, and GC. Based on these reports,[42] it is reasonable to expect that other boron-based bulky and weakly coordinating anions-based electrolytes hold promise in the development of Mg electrolytes[43] and Ca electrolytes.[44]

Despite recent advances on divalent metal electrolytes (Figure 2b and Table 1), most electrolyte systems cannot meet all performance metrics (Figure 2c), *i.e.*, high anodic stability at the cathode, high cathodic stability at the metallic divalent anode, high charge-transfer kinetics for both electrodes, and long-term cycling performance. To date, fluoroalkoxyborate-based Mg electrolytes show excellent anodic stability but insufficient cathodic stability due to a potential passivation film formed on Mg or Ca anodes. **DCC**-derived electrolytes and new electrolytes using the combination of simple Mg salt and special Mg additive (*e.g.* $MgCl_2$ and $Mg(BH_4)_2$, *etc.*) demonstrate sufficient cathodic stability, *i.e.*, the CE of Mg *plating/stripping* can reach 100%, but exhibit low anodic stability. Especially, the underlying fundamental reason for 100% CE and passivation-free characteristics are yet to be fully exploited in these systems. The bottom-up understanding of the interfacial charge-transfer during reversible Mg *plating/stripping* could allow us to rationally design an ideal electrolyte formulation that can meet requirements for both electrode sides in divalent metal batteries.

2.2. Solvation-dependent Stability

In most electrolytes for divalent battery systems, the solvation structure of active cation species can be easily altered by different donor oxygen/nitrogen denticity of solvents, strong coordination agents, and different Lewis acids, maintaining the dynamic charge equilibrium. Interestingly, the dielectric constant of a solvent is indirectly correlated to the solvation of Mg^{2+}.[31] Persson *et al.* examined a matrix of salt and solvent combination for potential Mg electrolytes, using combined classical molecular dynamics and first-principles simulations, and found Mg salts show a high tendency toward contact ion pair formation and aggregates in most organic solvents.[31,45] The solvation structure impacts not only the dynamics and charge transfer of active Mg species but also the stability of some anions[31,46] in the electrolyte, while there are many uncertainties in understanding the ion solvation structure from the computational study.[47] There exists a strong correlation between ion-pair formation and an increased tendency toward reduction of the anion (Figure 3a-b). At Mg metal anode potentials, the ion pair undergoes reduction at the Mg cation center, which can activate the anion for decomposition. Compared to ion pair-dictated decomposition of $TFSI^-$, a few anions, such as BH_4^-, Cl^- and BF_4^-, are stable against Mg metal reduction. Therefore, it is of fundamental importance to understand how different solvation structures in the forms of ion pairs (or active species) either incorporated with solvents are formed and being used for the electrochemical *plating/stripping* indeed, not just based on the developed salts itself. Accord-

Table 1. Summary of HOMO/IP and LUMO/EA energy levels and the corresponding redox potentials for the anion component and Coulombic efficiency for plating/stripping.

Mg electrolyte	Anion	HOMO [eV]	IP[e] [V vs Mg]	$U_{ox\text{-}expected}$ [V vs Mg]	$U_{ox\text{-}reported}$ [V vs Mg]	LUMO [eV]	EA[f] [V vs Mg]	$U_{red\text{-}expected}$ [V vs Mg]	CE [%]
DCC[11]	R'_yAlCl_{3-y} (R' = n-butyl and/or ethyl, y = 0–3)				2.2 (Pt)				100.0 (Pt, mass)[a] 99.6 (Pt, charge)[a]
APC[12]	$Ph_2AlCl_2^-$	−6.05		3.8		0.06		−2.3	
	$PhAlCl_3^-$	−6.40		4.2		−0.06		−2.2	
	Ph_4B^-	−4.82		2.6	2.6 (Pt)	−0.54		−1.7	
	$(C_6F_5)_3BPh^-$	−5.56		3.3	3.7 (Pt)	−0.42		−1.8	
HMDS $+AlCl_3$[14]	$(HMDS)_2AlCl_2^-$				3.2 (Pt)				95–100 (Pt)[b]
	$(HMDS)AlCl_3^-$ [58]	−5.67		3.4	3.9 (Pt)				99 (Pt)[b]
MACC[18a]	$AlCl_4^-$				3.1 (Pt)				98.8 (Cu)[c]
Carborane[23]	$HCB_{11}H_{11}^-$				4.6 (Pt)				> 99 (Pt)[b]
	$FCB_{11}H_{11}^-$				4.9 (Pt)				> 99 (Pt)[b]
Alkoxy-based		−5.00			3.5 (Pt)	2.70			> 98 (from 3rd, Pt)[d]
	B or Al $(OR^F)_4^-$ R^F = fluorinated alkyl group[34]				4.3 (SS/Al)				
	$B((CF_3)_4C_2O_2)_2$[41]				4.0 (Pt/SS/Ti/Al/GC)				95 (Pt)[b]
	TPFA in 3-methylsulfolane or G3[43a]				> 5.0 (SS, Al, Pt, Au, GC)				~96 (Pt)[b]
	$B(Hfip)_3$/Cl in DME[35]				~3.0 (Al) ~2.8 (GF) ~2.5 (SS)				~98.5 (Cu)[b]
$MgTFSI_2 + Mg(BH_4)_2$ or $MgCl_2$[31]	TFSI in AN		5.13		3.6		−1.47		
	TFSI in THF		4.94				−2.01		
	TFSI in G2		4.93		4.1		−2.05		
	BH_4 in THF		3.43		2.3		−3.08		
	BF_4 in AN		7.39		5.3		−1.74		
	BH_4 in DME[28]				~1.7 (Pt) ~2.2 (Au)				67 (Pt, Au)[b]
	TFSI/Cl in DME				> 3.0 (Pt)				~100 (after conditioning, Pt)[a,b,c]
$Mg(OTf)_2/MgCl_2$/DME	OTf/Cl in DME				1.9 (Al) 2.0 (SS) 2.4 (Ni) 3.1 (Mo)				89.9, 99.4 (1st, average, c-Al)[d]

[a] Calculated by EQCM method, [b] Caculated based on the charges passed in CV measurement, [c] Calculated based on the macro-reversibility measurement,[26b] [d] Calculated based on the galvanostatic plating/stripping, [e] Ionization Potential, [f] Electron affinity.

ingly, there have been great efforts to identifying the active species in the different electrolytes for divalent battery systems. As representatively sorted out in case of Cl^-, BH_4^-, and $TFSI^-$ anions along with some bulky anions as well, active species can dramatically change depending on the different combinations of anions/solvents even with an identical anion (*i.e.* Cl^-, BH_4^-, and $TFSI^-$) used.

2.2.1. Electroactive Species with Cl^-

Doe *et al.* filed a patent in 2013[48] on the addition of chlorides (*i.e.* $MgCl_2$) to the $Mg(TFSI)_2$ solutions (in **DME**), which can yield solutions that support highly reversible and stable Mg deposition. Later, this finding was further extensively studied with a new formulation ($Mg(TFSI)_2$_$2MgCl_2$ in **DME**)[26b] by a wide variety of analytical tools.[29b] Interestingly, $MgCl_2$ has very poor solubility in $Mg(TFSI)_2$/**G2** solutions and only moderate solubility in $Mg(TFSI)_2$/triglyme (**G3**) solutions. **DME**, as a bidentate ligand, strongly promotes the formation of divalent cations, such as $[Mg_2Cl_2]^{2+}$ and $[Mg_3Cl_4]^{2+}$, stabilized by intrinsically (or preferentially) bound **DME** molecules. The dramatic improvement in the electrochemical properties, driven by the addition of chloride anions into pristine $MgTFSI_2$ solution in **DME**, could be potentially attributed to weaker Mg ions-**DME** solvates, stabilized intermediates by ligand rearrangement, and barrier effect of Cl^-containing complexes at the surface to prevent decomposition of TFSI anion. This strategy has been extended to high concentration electrolytes of $Mg(TFSI)_2$:$MgCl_2$:2**TGM** for high-temperature applications.[49]

In the meantime, unique cation complex of $[Mg_2(\boldsymbol{\mu}\text{-}\mathbf{Cl})_2(\mathbf{DME})_4]^{2+}$ was identified for highly active electrolytes both from the experimental and theoretical analysis;[50] the cation complex can be formulated in **DME** by **dehalodimerization** of $MgCl_2$ through reacting with Cl^- ion acceptor or switcher (Figure 3c),[51] such as Lewis acid compound (*e.g.* $AlEtCl_2$ or

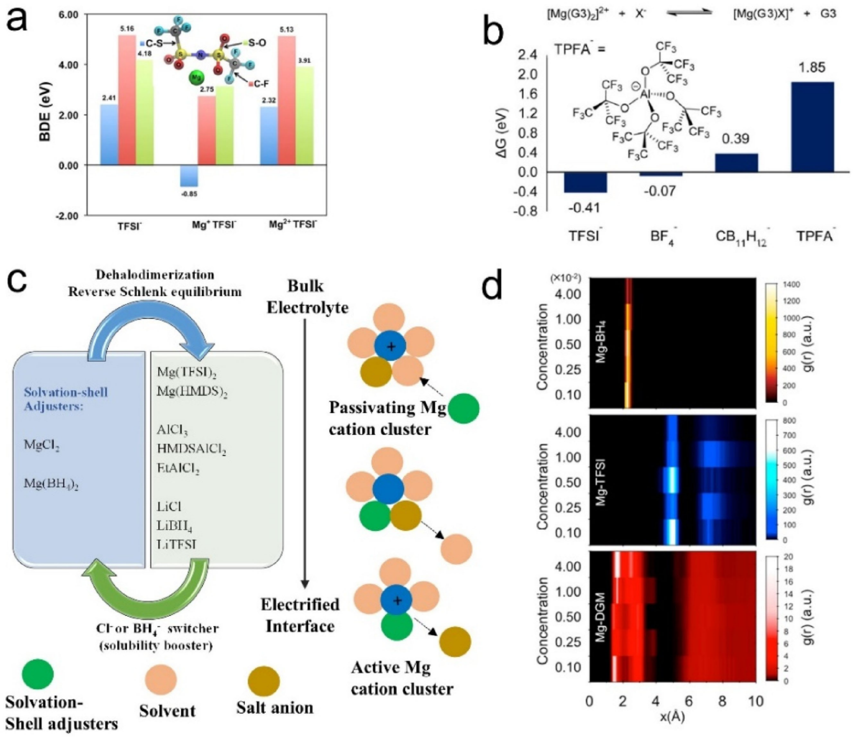

Figure 3. Tailored designs of the divalent cation solvation shell. a) bonding dissociation energy of $TFSI^-$ in different chemical environments corresponding to well-solvated, Mg^+ ion paired and Mg^{2+} ion paired configurations in a PCM model. Reproduced with permission from.[31] Copyright 2015 American Chemical Society; b) The computed free energy change in triglyme (G3) of ion association of various anions (X^-) with $[Mg(G3)_2]^{2+}$. A negative ΔG indicates favorable ion association and a positive ΔG indicates unfavorable ion association in G3. Reproduced with permission from.[43a] Copyright 2019 The Electrochemical Society. c) Successful electrolyte formulation with Cl^- and BH_4^- as solvation-shell adjusters. d) Radical distribution function of Mg–BH_4, Mg-TFSI, and Mg–G2 in a mixed solution of 0.01 M $Mg(BH_4)_2$/G2 with varying concentration of $Mg(TFSI)_2$. Reproduced with permission from.[57] Copyright 2018 Elsevier.

$AlCl_3$, *etc*)[52] and an Mg compound ($Mg(TFSI)_2$) that is solvable in **DME**. The overall reaction was driven by the ability of the acceptor or switcher to extract one Cl^- from $MgCl_2$ and/or the formation of the more stable dimer species. Such a reaction pathway was also recognized as the **reverse Schlenk equilibrium** (*i.e.* **comproportionation**),[53] where the solubility of $MgCl_2$ can be greatly enhanced in the Mg(**HMDS**)$_2$/**THF** system. Wang *et al.*[54] used the hard Lewis acid of Li^+ from the source of LiTFSI to enhance the Mg^{2+} active species concentration in the Mg(**HMDS**)$_2$ in **G4** electrolytes. Similarly, it was found that the hard Lewis acid of Li^+ from LiCl plays similar roles in the **MACC** electrolyte using **THF** as the solvent.[55] The **reverse Schlenk equilibrium** was also successfully applied to enhance the solubility of Mg(**HCB$_{11}$H$_{11}$**)$_2$ in **DME** by reacting with $MgPh_2$.[21] Through the above mechanism by increasing the solubility of electrolyte agents (*i.e.* $MgCl_2$ or $Mg(BH_4)_2$), the (first) solvation structure of bulk electrolytes, significantly altered from the active cation species, are vulnerable to be reduced on the Mg metal anodes. Besides, the agent anion species are stable against the reduction environment. At the electrified electrode surface, the modified speciation of solvation structure involving the solvation-shell adjusters (*i.e.* Cl^- or BH_4^-) releases the weakly coordinating anions or solvents and secure the reductive stability as well as suppressing the detrimental formation of passivation layers. However, it is noted that such solvation-shell adjusters in the bulk electrolytes are not typically designed for high anodic stability, which requires further solvation engineering for the practical realization of divalent battery systems.

More recently, Mg triflate was utilized with either $MgCl_2$/$AlCl_3$ or $MgCl_2$ in **DME**. The former involves the similar active cation species of [Mg$_2$(**μ-Cl**)$_2$(**DME**)$_4$]^2 and $[(OTf)AlCl_3]^-$ formed through dehalodimerization and Lewis acid-base reactions, which are further decomposed during the electrolyte conditioning.[56] However, such Cl-based active species are unlikely to form in the latter, and Mg(**DME**)$_2$(OTf)$_2$ and Mg-OTf ion pair exist instead due to the high $[Mg^{2+}]/[Cl^-]$ ratio and highly delocalized character of OTf^- anion with a smaller size than $TFSI^-$.[27]

2.2.2. Electroactive Species with BH_4^-

As a halide-free anion example, BH_4^- has been extensively studied for divalent electrolytes. The solvent can exert a substantial impact on the effective concentration of Mg active species with BH_4^-.[28] Especially, the 0.1 M $Mg(BH_4)_2$ in **DME** possesses a higher concentration and faster mobility of Mg active species, compared to those in 0.6 M $Mg(BH_4)_2$ in **THF** (Figure 4a). Despite the lower concentration in **DME**, the Mg *plating/stripping* kinetics was greatly enhanced, and the CE was increased from 40% to 67% calculated by CV method. As

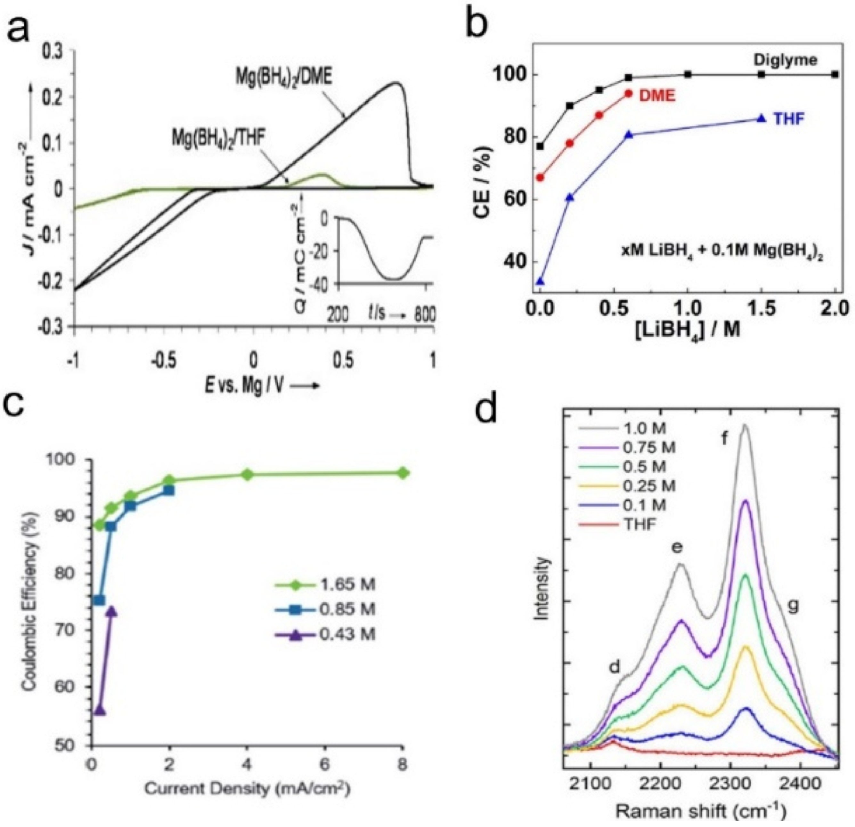

Figure 4. Interplay between electroactive species concentration and charge-transfer kinetics. a) Cyclic voltammogram for 0.1 M $Mg(BH_4)_2$/DME compared to 0.50 M $Mg(BH_4)_2$/THF. Inset shows deposition/stripping charge balance for Mg(BH4)2/DME. All experiments used Pt working electrodes and Mg reference/counter electrodes. Reproduced with permission from.[28] Copyright 2012 Wiley-VCH; b) The CE of Mg plating/stripping of investigated electrolytes: 0.1 M $Mg(BH_4)_2+LiBH_4+$solvent and the concentrations of $LiBH_4$ $x=0$–2.0 M. Reproduced with permission from.[29a] Copyright 2013 Springer Nature Limited; c) Average CE values measured during galvanostatic Ca plating/stripping at a Au electrode as a function of current density and $Ca(BH_4)_2$ concentration in THF. Reproduced with permission from.[59] Copyright 2020 The Royal Society of Chemistry; d) Raman spectra of $Ca(BH_4)_2$ in THF at different concentrations in regions 2060–2450 cm^{-1}. Reproduced with permission from.[60] Copyright 2019 American Chemical Society.

complete dissociation of $Mg(BH_4)_2$ into discreet ions is unlikely, $Mg(BH_4)_2$ exists as the contact ion pair $[Mg(\boldsymbol{\mu}\text{-}\mathbf{H})_2\mathbf{BH_2}]_2$, which partially dissociates into $[Mg(\boldsymbol{\mu}\text{-}\mathbf{H})_2\mathbf{BH_2}]^+$ and BH_4^-; the dissociation degree depends on the solvent and other salt additives. The nuclear magnetic resonance (NMR)/infrared spectroscopy (IR) analysis indicate that the interactions between Mg^{2+} and BH_4^- is weaker in **THF** and the salt dissociation of the $Mg(BH_4)_2$ is thus stronger in the electrolyte using **DME** as solvent (albeit **DME** has a slightly lower dielectric constant (7.2) than **THF** (7.4)). Further, $LiBH_4$ was proposed as a promoter to enhance the solubility of $Mg(BH_4)_2$ in **DME**. The resultant CE was found to be proportional to the molar ratios of $LiBH_4/Mg(BH_4)_2$.

Diglyme as a tridentate (three oxygen atoms) solvent ligand can drastically enhance the coordination with Mg^{2+} in a favorable kinetic way (Figure 4b).[29a] The formulation of 0.1 M $Mg(BH_4)_2$_1.50 M $LiBH_4$ in **G2** can render the CE of Mg *plating/stripping* almost close to 100 % on Pt substrate calculated by CV method. As a new alternative approach, the mixture of $Mg(TFSI)_2$ and $Mg(BH_4)_2$ in a molar ratio of 4:1 can significantly influence the coordination environment of Mg^{2+} in **G2**,[61] *i.e.*, changing the first solvation shell from $[Mg(TFSI)(\mathbf{G2})_2]^+$ to $[Mg(TFSI)(BH_4)\mathbf{G2}]$, which is consistent with the solvation structure derived from ^{25}Mg NMR studies (Figure 3c, d).[57] Under this solvation structure, more **G2** solvent can be released to increase the solubility of $Mg(BH_4)_2$ salt.

It is well-accepted that BH_4^- is a stronger coordinating ligand and forms stable ion pairs even at a very low concentration (0.01 M). The strategy of disrupting the rigid solvation structure between divalent metal ions (Mg^{2+} and Ca^{2+}) and BH_4^- can be realized through the addition of a competitive additive (ligand species), which can preferentially interact with Mg^{2+} or BH_4^- to release more solvent from the first solvation shell. A promising additive of tris(2H-hexafluorisopropyl)borate (**THFPB**) has been demonstrated due to its preferential coordination with BH_4^-.[62] With the aid of the strong electron-acceptor ability of the **THFPB** additive, a higher concentration (0.5 M-almost 50 times higher than that of pristine $Mg(BH_4)_2$/**G2** electrolytes) of $Mg(BH_4)_2$ has been achieved.[62] In another study, PEGylated-ionic-liquids were reported to preferentially coordinate with Mg^{2+} through the presence of polyether chains, which can drastically enhance the solubility of $Mg(BH_4)_2$ to 0.5 M and thus change the solvation structure initially based on BH_4^-.[30a] Jiao *et al.* recently[63] revealed that the addition of $LiBH_4$ into $Ca(BH_4)_2$-**THF** electrolyte can significantly reduce the coordination number of oxygen in the first solvation shell of Ca^{2+}, *i.e.*, the releasing solvent of **THF** (*i.e.* Li^+ has a higher coordination capability toward **THF**), and then decrease the solvation energy of Ca^{2+}, which enables a facile de-solvation process and a fast charge-transfer process during Ca *plating/stripping* at room-temperature as further supported by computations.

In the study of a simple electrolyte system of $Ca(BH_4)_2$/**THF**, Zavadil *et al.*[59] gained important insight into the role of the liquid solvation environment in facilitating the reversible electrodeposition of divalent metal (Figure 4c). Their results show increasing salt concentration (*i.e.* 0.43 M to 1.65 M) and decreasing cation charge density (*i.e.* from Mg^{2+} to Ca^{2+}) can tune solution speciation from uncharged neutral species toward multimers and ionic clusters, capable of delivering Ca^{2+} at appreciable rates, while sparing parasitic loss from electrolyte decomposition. This finding in the high-concentration regime (*ca.* 1.65 M) should be associated with the less participation of solvent in the first solvation shell, which also holds true for other alkali metal systems. In the high-concentration regime, Gewirth *et al.*[60] demonstrated the areas of B–H stretching mode show a linear increase with increasing concentration of $Ca(BH_4)_2$ in **THF**, but not for the band of three B–H stretching modes in Raman spectra (Figure 4d). This observation indicates that BH_4^- anions are present in the solution but do not interact strongly with the Ca^{2+} cations. The Ca^{2+} cations are found to be primarily solvated by **THF** solvent but interact weakly with the BH_4^- anions in other Raman spectra. Overall, the Ca^{2+} in the $Ca(BH_4)_2$/**THF** system shows an analogous solvation environment as $Li^+/Na^+/K^+$ in their high-concentrated salt system. In a comparative study using $Mg(BH_4)_2$ and $Ca(BH_4)_2$ in **THF**, it is found that the latter contains more metal-BH_4^+ species for high Coulombic efficiency electrodeposition while the former remains neutral monomers in a wide range of salt concentrations from combined experiments and computational simulations.[64]

2.2.3. Electroactive Species with $TFSI^-$

$Mg(TFSI)_2$ is an ether-soluble "simple" Mg salt. The poor electrochemical performance of Mg electrodes in its solutions hinders its practicality as a viable electrolyte for Mg batteries.[65] The concentration and the solvent media can greatly impact the local coordination environment of Mg^{2+} and thus the Mg *plating/stripping* behavior.

Choi *et al.*[66] firstly investigated electrolyte formulations of $Mg(TFSI)_2$/glymes and found 0.3 M $Mg(TFSI)_2$ in **DME**/**G2** (1/1, v/v) shows the optimum electrochemical performance with excellent anodic stability exceeding 4.0 V with Al or stainless steel (SS) working electrodes. The $Mg(TFSI)_2$/**G2** electrolyte was systematically studied in the concentration range of 0.1–1.5 M.[26a] The poor electrochemical performance was observed in all concentrations with large onset overpotential for Mg *plating/stripping* and low CE. Mg cation transference number (t^+) decreases from 0.297 to 0.036 as electrolyte concentration increases from 0.2 M to 1.50 M. Such a difference in t^+ is attributed to the difference in ion mobility. At higher concentrations, the coordination environment of Mg^{2+} species is greatly changed. Shielding effects from anions to the active cation species containing Mg^{2+} become more prominent at higher electrolyte concentrations, which results in a more limited cation mobility. The $t^+ = 0.141$ of $Mg(TFSI)_2$/G2 at 0.5 M is comparable to the halogen contained electrolytes, where thereof t^+ is between 0.13 (DCC) and 0.159 (APC). This finding suggests dissociation of anions in electrolyte dominantly contributes to the current flow, since the most of bulky anions at the high concentration regime retard the diffusion of Mg^{2+} or active cation species.

A unique behavior of $Mg(TFSI)_2$/**DME** was reported,[67] where phase separation occurs for electrolytes with the concentration between 0.05 M to 0.35 M. The electrolyte is homogenous below 0.05 M and above 0.35 M up to 1.25 M, which should be associated with diverse conformers in the **DME** solvent.**[68]** Recently, a new approach was realized by the addition of secondary dimethylamine (**DMA**) solvent (cosolvent system) into the $Mg(TFSI)_2$/**THF**-glymes system.[69] **DMA** can increase the solubility of $Mg(TFSI)_2$ in **THF** solvent and their experimental results show the **DMA** can participate in the first solvation shell of Mg^{2+} with **THF** and a $TFSI^-$ anion, compared to two $TFSI^-$ anions in the pristine solvation shell of Mg^{2+} dissolved in **THF**, which accordingly dissociate the coordination between $TFSI^-$ and Mg^{2+}. Uchimoto *et al.*[70] studied the solvent dependence of $Mg(TFSI)_2$ on the alloying reaction with bismuth (Bi). In the 0.50 M $Mg(TFSI)_2$/**AN**, the alloy reaction took place, whereas the alloying reaction did not occur in 0.5 M $Mg(TFSI)_2$/2-methyltetrahydrofuran (**2-MeTHF**) due to the different coordination structure of $[TFSI]^-$ in both electrolytes. Raman study shows less than 15% of $TFSI^-$ coordinate with Mg^{2+} in 0.50 M $Mg(TFSI)_2$/**AN** but more than 90% of $TFSI^-$ coordinates with Mg^{2+} in 0.50 M $Mg(TFSI)_2$/**2-MeTHF**. The coordinated $TFSI^-$ undergoes reduction decomposition more easily than free $TFSI^-$.[31,70] Thus, the excessive decomposition products of $[TFSI]^-$ on the surface of the electrode are supposed to inhibit the insertion of Mg^{2+} to the Bi electrode. Selection of solvent or mixed solvents is thus demonstrated to render a great impact on the reversibility of Mg *plating/stripping* for $Mg(TFSI)_2$-based Mg electrolytes,[71] while intrinsic chemical instability of Mg anodes with $Mg(TFSI)_2$ and glymes has been raised from experimental and theoretical basis.[72]

Recently, from the comprehensive study on the correlation of anion association strength and electrochemical response, it is established that cooperative effects of anions critically dictate the deposition/dissolution overpotentials in a variety of divalent metal batteries.[73] Besides, strongly coordinated ethereal solvents (*e.g.* **DME**, **G3**, etc.) to Ca^{2+} rather inhibit the reversible calcium deposition due to the destabilized solvents or frustrated Ca^{2+} desolvation.[74]

3. Interfacial Dynamics

3.1. Molecularly Defined Electrode Surface Layer

3.1.1. Impact of Impurities

Compared to extensive studies on the surface chemistry of alkali metals, understanding of the complex surface chemistry on the Mg or Ca metal surface is still in scientific immaturity. On the alkali metal surface (in contact with proper electrolyte), a stable SEI film is formed, which allows alkali metal ions to transport but blocks electron transfer. However, divalent metal cation electrolytes need a totally different mechanism for Mg and Ca *plating/stripping* such that impurities in the salt or solvent, can greatly change the surface chemistry of fresh divalent metal electrodeposits. It was revealed that the profound impact of trace levels of H_2O ($\leq$ 3 ppm) on the kinetics of Mg *plating* and determined that passive film of MgO and $Mg(OH)_2$ are formed only after Mg *plating* ceases,[75] rather than continuously during Mg *plating*. The inhibition of this passivation by Cl^- derives from the formation of adsorbed Cl^- and/or $MgCl_2$ on the surface, as well as a dynamic competition with H_2O in the double layer. Meanwhile, using a high purity LiTFSI, instead of $Mg(TFSI)_2$, the LiTFSI/$MgCl_2$/**DME** (analogous system to $Mg(TFSI)_2$/LiCl/**DME**) solutions can enable Mg *plating/stripping* cycling efficiency to reach 100% which is calculated by more rigorous macro-reversibility measurements along with electrochemical quartz crystal microbalance (EQCM) and CV method.[26b] The limited amount of research results in the literature indicate a trace amount of impurities in the electrolytes have a drastic influence on divalent metal electrochemistry. In the meantime, surface impurities of naturally occurring passivation layers (*i.e.* MgO) on Mg anodes significantly affected the diffusion of magnesium ions or the adsorption behavior of cationic species, while recent pretreatment by a titanium complex ($Ti(TFSI)_2Cl_2$)) resulted in a fresh Mg surface for reversible and stable Mg *plating/stripping*.[76]

3.1.2. Participation of Cl^-

Matsui *et al.* proposed an ***operando*** Fourier-Transform Infrared Spectroscopy (FTIR) method to study the evolution of surface layer during cyclic voltammetry (CV) sweeping in the two representative electrolytes;[77] one is organohaloaluminate-based **EAC** electrolyte (0.25 M $EtMgCl–2Et_2AlCl$ in **THF**); the other is a typical ionic **BuMeG3** electrolyte (0.50 M $Mg(TFSI_2)$ in butyl methyl triglyme). A diamond attenuated total reflection (ATR)-based *in situ* FTIR cell was employed to collect FTIR spectrum in the single beam mode. The evolution of species on the working electrode (Pt) can be easily identified by the corresponding negative or positive peaks in the spectra. The surface layer using **EAC** electrolyte is revealed to base upon adsorption or a structural reformation of the **THF** molecules at the vicinity of the electrode. Since this surface layer is not formed by the irreversible decomposition of the electrolyte formulation, the **EAC** electrolyte maintains dynamic reversible interphase. Besides, the effect of chloride content on electrolyte chemistry, the microstructure, and the surface chemistry of electrodeposited Mg was systematically studied using different analytical methods.[78] Three different electrolytes were chosen, *i.e.*, Mg aluminum chloride complex (**MACC**: $MgCl_2 + AlCl_3$) with the highest chloride content, Mg triphenoxyaluminate (**MTPA**: $PhMgCl + Al(OPh)_3$ in 4:1 ratio), and **TFSI** ($Mg(TFSI)_2$ in **G2**) with no chloride. The microstructure and chemistry of the Mg films, along with their overall cycling efficiency, showed a strong dependence on chloride contents in the electrolytes. The films formed with the higher chloride concentration electrolytes (**MACC** and **MTPA**) yielded large and columnar grain structures with a strong [0001] texture. However, **TFSI** electrolyte yields taller and narrower crystals and promotes growth with a $[2\bar{1}\bar{1}0]$ and [0001] direction. Higher levels of impurities were observed in electrodeposited Mg in conditioned **TFSI** electrolyte relative to conditioned **MACC** and **MTPA**, indicating lower electrolyte stability and improved protection of freshly deposited Mg metal by chloride species.

The degradation mechanisms of an Mg metal anode in a 0.3 M $Mg(TFSI)_2$_0.15 M $MgCl_2$ **G2** electrolyte was reported at a current density (1 $mA\,cm^{-2}$) and an areal capacity (0.4 $mAh\,cm^{-2}$).[65] The passivation layer on the Mg metal surface is possibly composed of various decomposition products of $TFSI^-$ anions, chlorides, and a trace amount of H_2O. In a similar system, it was speculated that the bare metallic Mg electrode can spontaneously react with $TFSI^-$ anions to generate unstable layers.[29b] The excess of Cl^- containing complexes resides near or at the anode, possibly acting as an adsorbate layer, which can keep the $TFSI^-$ anion from reaching the reduced Mg surface and facilitate the removal of passivating oxides in case they form. It is plausible that reactions similar to corrosion, mediated by Cl^- anions, assist in dissolving away passivating surface films on Mg metal, such as $MgO/Mg(OH)_2$ layers.

Similar to $MgCl_2$, $CaCl_2$ has been proposed as a surface film in the early Ca primary batteries.[79] $CaCl_2$ is mostly an anion (Cl^-)-conductor ($t^+ = 0.1$). Presumably, the electrolyte-facing redox step upon Ca stripping involves precipitation of $CaCl_2$, while the Ca-facing redox process involves the reduction of non-mobile Ca^{2+} within $CaCl_2$ lattice (Note that plating has not been demonstrated practically with $CaCl_2$; the reverse stripping/corrosion process predominates in Ca primary batteries). Thus, a dynamic chemical precipitation/dissolution occurs upon Ca stripping in the early reported Ca primary batteries, however, which cannot make Ca batteries rechargeable.

More strongly coordinating Cl^- anion lowers the dissolution overpotential due to the higher driving force for re-solvating divalent cations into the Cl-rich coordination environment.[73] However, the strong adsorbate layer might increase the plating overpotential instead by disturbing the diffusion of active cation species through this layer as well as the reduction of $TFSI^-$ anion. Therefore, the use of cooperative anions such that both plating/stripping overpotentials can be reduced is highly desirable while improving the compatibility with potential oxide cathodes by lowering or eliminating the corrosive Cl^- anions in the electrolytes.

3.1.3. Participation of BH_4^-

Another anion-conductors, like CaF_2 and CaH_2, have been observed in recently reported Ca systems.[2a] The first reversible Ca deposition on Cu at elevated temperature (75-100 °C) was demonstrated in 2016.[80] The optimized electrolyte formulation was 0.3 M $Ca(BF_4)_2$ in **EC**(ethylene carbonate):**PC**(propylene carbonate) (1:1 v/v), which could render the maximum Ca^{2+} mobility by minimizing BF_4^- in the Ca^{2+} first solvation shell. The surface layer formed on deposited Ca was determined by X-ray powder diffraction (XRD) to be CaF_2, along with solvent-derived organic phases identified by FTIR. However, the origin of CaF_2 is still unknown. The investigation of Ca^{2+} electrolyte in ether-based solvents showcased in 2018 reported highly reversible Ca plating in 1.5 M $Ca(BH_4)_2$ in **THF** using a gold (Au) working electrode at room temperature.[81] The electrolyte was reported to react quickly with deposited Ca to generate exclusively CaH_2 as the **SEI** (Figure 5a). It was deduced that the origin of electrolyte component forming CaH_2 was likely **THF** rather than BH_4^- based on their gas chromatography-mass spectrometry measurements. However, attempts on using $Ca(TFSI)_2$/**THF** were unsuccessful, indicating **THF** alone is insufficient to enable cycling but BH_4^- has a peculiar role.

Recently, the role of BH_4^- in this system was proposed that Ca deposition takes place through a chemical-electrochemical mechanism,[60] in which chemical H abstraction from BH_4^- in the bulk electrolyte and surface H adsorption precedes subsequent reduction of Ca^{2+}. Strong evidence of the proposed abstraction comes from liquid injection field desorption ionization (LIFDI)-MS measurement, which indicates a significant presence of BH_3·**THF** remains in the solution. It should also be noted that, so far, Ca deposition from $Ca(BH_4)_2$ in **THF** has only been reported on precious metal surfaces (Au or Pt), which may be necessary for the initial H surface adsorption (Figure 5b). Besides, in other systems like $Ca(B(\textbf{hfip})_4)_2$/DME,[38–39] the formation of CaF_2 is the result of chemical reduction of the hexafluoroisopropoxy ligand at the highly reducing potential of Ca metal. Less CaF_2 is observed than that in $Ca(BF_4)_2$ in **EC/PC**.[80] The solid evidence on the presence of CaH_2 and CaF_2 on new electrodeposited Ca may render a different interface charge-transfer route for Ca *plating/stripping*, which mainly rely on the migration ability of X^- anions (H^- and F^-, Figure 5c), compared to the SEI film relying on Li^+ migration for Li *plating/stripping* (Figure 5d).

3.1.4. Artificial Films

For the Li-ion chemistry, the electrolytes are irreversibly reduced on the electrode surface (*i.e.* SEI layer) which enable the Li-ion conduction through this passivating film. However, it is widely accepted that such passivating films are incapable of enabling the reversible electrochemistry of divalent metal anodes due to the sluggish diffusivity of divalent metal cations. Recently, the feasibility of constructing Mg^{2+}-conducting artificial films on an Mg anode has attracted attention. An Mg^{2+}-conducting (1.19×10^{-6} S cm^{-1}) and electronic-insulating (1.04×10^{-7} S cm^{-1}) artificial polymeric interphase (100 nm) was engineered on the Mg anode surface,[82] which enabled high reversible Mg electrochemistry in carbonate-based electrolytes. Inorganic compounds such as MgI_2 (*ca.* 120 Ω)[83] or MgF_2 (1022 Ω; < 200 nm)[84] were introduced on the surface of the Mg anode to provide Mg^{2+} conducting layers. Similarly, a Sn-based artificial film was formed *via* ion-exchange and alloying reactions (0.15 M $SnCl_2$ in **DME**) onto Mg metal anode,[85] which can drastically reduce the interfacial resistance of Mg (from 450 KΩ to 10 KΩ) in the simple ionic electrolyte of $Mg(TFSI)_2$/

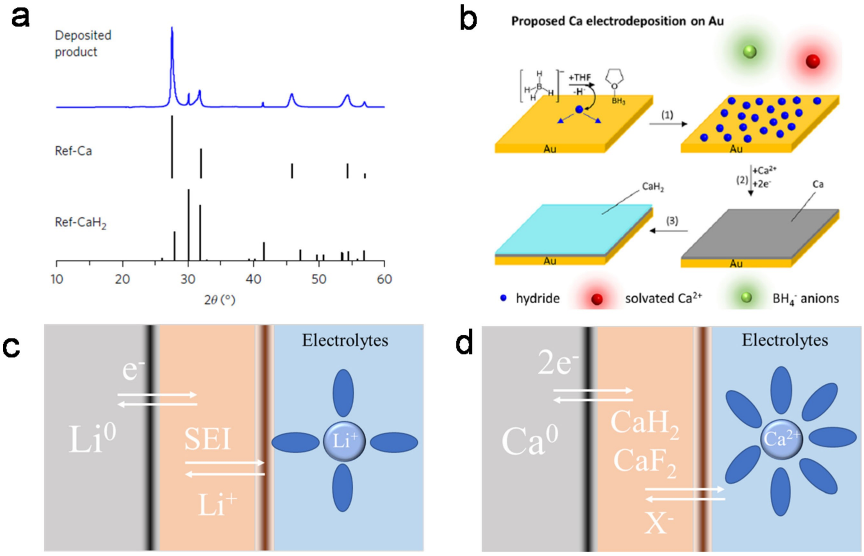

Figure 5. Proposed charge-transfer routes for Ca metal plating/stripping. a) Characterization of the product formed on Ca plating using the $Ca(BH_4)_2$/THF. Powder XRD patterns showing the dominant product on plating is Ca with a small amount of CaH_2. Reproduced with permission from.[81] Copyright 2017 Macmillan Publishers Limited; b) substrate dependence of Ca plating in the $Ca(BH_4)_2$/THF. Reproduced with permission from.[60] Copyright 2019 American Chemical Society; Schematic representations of the interphase charge-transfer route for active Li species based on SEI model (c) and Ca species (d) based on CaX_2.

DME. Cui *et al.*[86] reported a novel method of generating a stable artificial film by the partial decomposition of a pristine Li electrolyte (Li[B(**hfip**)$_4$]/**DME**) on the Mg metal, after which Mg^{2+} is directly introduced into this electrolyte to form a hybrid Mg^{2+}/Li^{+} conducting film (*ca.* 500 Ω vs. 20 KΩ prior to Mg^{2+} incorporation). By introducing $GeCl_4$ into the ether-based electrolytes, Ge-based multicomponent layers *in-vivo* protect the Mg anode over the prolonged cycles.[87] As long as the artificial interphase on the Mg anodes is robust and Mg^{2+}-conducting,[88] it can be a universal strategy to modify the interface chemistry of Mg anodes while preventing the detrimental surface passivation from decomposition reactions of various electrolytes components.

The charge-transfer route and kinetics of divalent metal *plating/stripping* are strongly dependent on the different types of electrolytes. Generally, Cl^- or BH_4^--containing electrolytes have been reported by adsorption-dissolution-deposition route;[3b,60–61, 89] agent-free electrolytes have been reported to influence the kinetics by the mole concentration of electroactive divalent metal ion species and the participation of anions in the first solvation shell.[26a,59, 69]

3.2. Origins of Electro-conditioning

It is often reported that high CE and low overpotentials of Mg *plating/stripping* are achieved from Mg electrolytes only after the so-called "conditioning" cycles. In Al-free electrolytes, such as $MgTFSI_2/MgCl_2$ (1:2) in **DME**, for instance, the "conditioning" of the electrolyte primarily refers to an electrochemical removal of reductive impurities, for example, the trace amount of moisture, oxygen, and HTFSI. It was suggested that the conditioning process requires the passage of reductive faradaic currents associated with substantial charge passage, and therefore the negative scan should be span beyond the overpotential for Mg deposition.[26b] This "conditioning" procedure affects only the electrolyte solution, and it is not associated with any pretreatment of the electrodes.[36,71] Especially, the irreversible cathodic processes, associated with the contaminant, cannot form an insoluble surface film that fully blocks the surfaces of the electrode for any Mg deposition. In these electrolytes, the "conditioning" can thus be mitigated by adding small amounts of chemically reducing species, such as Bu_2Mg.

In Al-containing electrolytes, such as $MgCl_2/AlCl_3$-based solutions, it has been reported that the "conditioning" of the electrolyte is associated with Al deposition.[90] Thereby, a decrease of the Al/Mg ratio in the electrolyte, due to Al depletion and additional Mg *stripping*, and the formation of free Cl^- anions are theoretically predicted.[91] A multi-technique characterization approach was employed to reveal that the conditioning process involves increasing the concentration of the dimmer of $[Mg_2(\mu\text{-}Cl)_3\cdot 6\mathbf{THF}]^+$ in conjunction with the formation of free Cl^- in solution.[92] As both the increased concentration of Mg species in the electrolyte and the presence of Cl^- at the Mg anode are considered beneficial for lowering the overpotentials for Mg *plating/stripping*, such speciation is considered as an additional process during the "conditioning" of the electrolyte. However, as the depletion of Al associated with the dissolution of Mg has also been evidenced by stirring Mg powder in solutions of $AlCl_3/CrCl_3$,[93] or $MgCl_2/AlCl_3$ in ethers,[94] the process might proceed already in the absence of applied external voltage or current. In any case, it is discussed controversially if Al deposition originates from cationic Al moieties,[90] from anionic $AlCl_4^-$,[92] or neutral $AlCl_3$ species.[94]

Recently, as studied on the "conditioning" mechanism of $MgCl_2/AlCl_3$ and Mg(**HMDS**)$_2$/$AlCl_3$ in **TEGDME**-based electrolytes,[95] it is experimentally revealed that cationic $AlCl_2^+$ species in TEGDME-based electrolyte with an $AlCl_3/MgCl_2$ or $AlCl_3/MgHMDS_2$ ratio higher than 1:1 can corrode Mg metal by the cementation reaction mechanism. The suppression of the cationic $AlCl^{2+}$ species can be achieved by the desired stoichiometries or the adjuster of $MgCl_2$[95] or Mg powder[94] to make solvent-dependent active Mg speciation.

3.3. Surface Adsorption and Interfacial Charge Transfer

Mg *plating/stripping* is not a simple exchange of Mg^{2+}/Mg couple, rather it is controlled by adsorption of complexes in the halide-containing electrolytes of (i) Grignard-based electrolytes or inorganic electrolytes (*e.g.* **ACC**, **MACC**, $MgCl_2$-based electrolytes) or (ii) BH_4^--containing electrolytes (*e.g.* $Mg(BH_4)_2$-based electrolytes). (i) First, quantitative analysis using EQCM in Grignard-based electrolytes demonstrates such a complex adsorption process. Aurbach *et. al.* carried out the potentiodynamics of Mg *plating/stripping* in the **ACC** electrolytes on microelectrodes using EQCM.[96] Electroactive Mg cationic species, such as $Mg_2Cl_3^+\cdot 6\mathbf{THF}$ or $MgCl^+\cdot 5\mathbf{THF}$, approach the anode upon cathodic polarization, while Al anionic species are expelled out from the anode. Neutral Al species may play an important role during the Mg electrodeposition as the Cl^- ligand acceptor, while additional $MgCl^+$ has a similar role. EQCM studies of Mg *plating* revealed that at the onset of the cathodic reduction (less than 0.5 C mol^{-1}), the mass change per electron equivalent (**mpe**) is 27 g mol^{-1}, much higher than that for simple Mg^{2+}/Mg reaction (12 g mol^{-1}) which signifies the adsorption of complexes rather than Mg^{2+}. The **mpe** value of 27 g mol^{-1} can be rationalized by adsorption processes of neutral Al-based moieties and complex Mg–Cl-**THF** cations which accompany the electron transfer to the Mg ions. A second electron transfer, probably to adsorbed intermediate species produced in the first electron transfer, results in reduced Mg atoms and chloride anions in the solution phase (these interact with fresh Mg or Al species as suggested before) (Figure 6a).[3b] The reduced Mg atoms diffuse on the surface to form Mg nuclei, which might be connected to kink sites. The strong evidence for facile lateral diffusion of Mg adatoms is the near-perfect Mg microcrystals.[3b]

Qualitative analysis of the adsorption of complexes has been conducted using *in situ* FTIR to confirm the adsorption of RMg^+ or RMg· species on the Mg electrode's surface in three typical Grignard systems, namely, RMgX, $Mg(Al_{3\text{-}n}R'_nR'^{\prime\prime}_n)_2$, and $Mg(BPh_2Bu_2)_2$ solutions in the **THF**.[97] In the case of the $Mg(AlCl_{4\text{-}n}R_n)_2$ complex solutions, species such as $Mg_xCl_y^+$ may

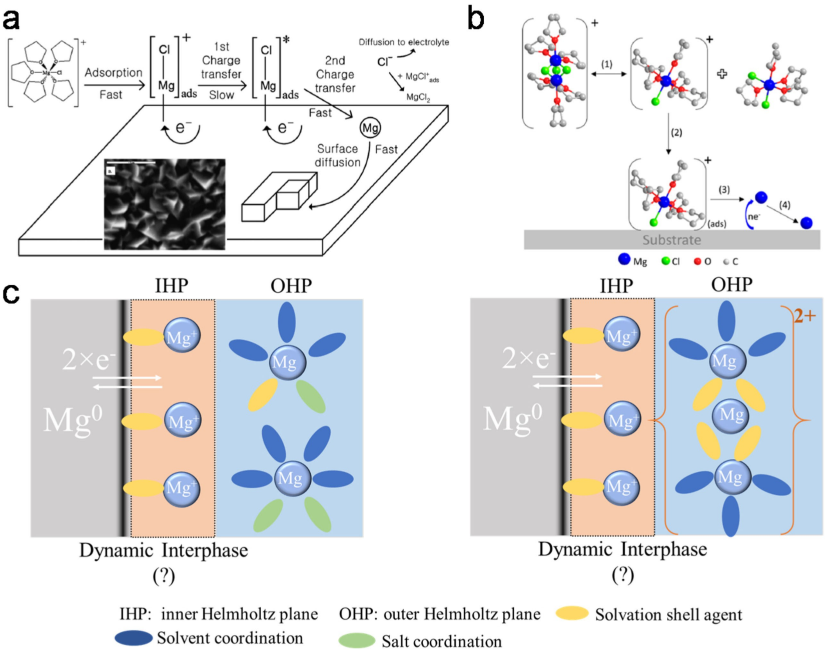

Figure 6. Proposed charge-transfer routes for Mg metal plating/stripping. a) Possible Mg-electrodeposition mechanism from complex ethereal electrolyte solutions. Reproduced with permission from.[3b] Copyright 2013 The Royal Society of Chemistry; b) Mg deposition is proposed to go through a chemical-electrochemical mechanism that involves (1) dimer $[Mg_2(\mu\text{-}Cl)_3\cdot 6THF]^+$ cation disproportionation. The cationic Mg species is adsorbed on the substrate surface and loses its ligands at more negative potentials (2). Adsorbed Mg^{2+} cations are further reduced (3) to form a crystallized Mg layer (4). Reproduced with permission from.[89] Copyright 2018 American Chemical Society; c–d) schematic representations of the interphase charge-transfer route for active Mg species from representative successful electrolyte formulations.

be adsorbed, in addition to species with Al–Cl and Mg–C bonds. In the case of the $Mg(BPh_2Bu_2)$ solutions, adsorbed species are likely $PhMg^+$ and $B(Ph_2Bu_2)Mg^+$. All the above species are probably stabilized by **THF** molecules that are coordinated by Mg ions. Recently, Gewirth *et al.*[89] employed the CV and LSV (linear sweep voltammetry) with an ultra-microelectrode to study the mechanistic pathways of Mg plating in the same electrolyte and proposed a chemical-electrochemical mechanism, where a chemical step is involved by the dimer $[Mg_2(\boldsymbol{\mu}\textbf{-Cl})_3\cdot 6\textbf{THF}]^+$ cation disproportionation reaction (Figure 6b).

In another study, *in situ* XRD, XPS, SEM (scanning electron microscope), and electrochemical methods were used to interrogate the mechanism of Mg electrodeposition from PhMgCl/$AlCl_3$ and EtMgCl electrolytes.[98] An open circuit potential (OCP) pause, following Mg deposition, enhanced Mg *plating/stripping* kinetics along with lowered overpotentials for both plating and stripping. The improvement is attributed to an "enhancement layer" that is formed on the electrode during the OCP hold, which consists of Mg and Cl on the electrode surface, possibly following electrode de-passivation. The electrochemical deposition of Mg from $[Mg_2(\boldsymbol{\mu}\textbf{-Cl})_3\cdot 6\textbf{THF}]^+$ was monitored through *in situ* potentiostatic X-ray absorption spectroscopy (PXAS) of the Mg K-edge.[99] X-ray absorption near-edge structure, XANES, is an element-specific process that empirically determines the oxidation state of the absorbing species.[100] Further, developed *in situ* electrochemical XAS cells enabled to make this fundamental study feasible.[101] Initially, it was observed that the size of the wave increases and the edge energy decreases in the XANES upon applying lower potentials.[99] The presence of a XANES signal, prior to the onset of Mg deposition, indicates the presence of a new Mg species near the Mg-dimer. Later, they performed the *in situ* analysis of the extended X-ray absorption fine structure (EXAFS) region.[102] The Fourier-transformed EXAFS spectra show a shift of the first-shell peak, which can be interpreted as a significant decrease in the first-shell scattering distances around Mg at the interface, *i.e.*, the formation of an intermediate species from the dimer in the bulk electrolyte (Figure 7a). Recently developed in-situ/operando XAS analysis showed great promise to identify the interfacial species at different potentials.[103]

It was predicted that the strongest adsorbing species at the Mg interface are $MgCl^+$ complexes, which are also the active species involved in the charge transfer.[104] Especially, the energy to (de)solvate $(MgCl)^+$ is minimal. Levi. *et al.* systematically studied the kinetics of all-inorganic, Cl-containing complex $MgCl_2$:$AlCl_3$ (1:1) complex compound, all-organic Bu_2Mg with different ratios of Bu_2Mg, and various combinations of $AlEtCl_2$ and $AlEt_3$.[105] The exchange current density of Mg deposition increases considerably as the organic ligand/Cl-ligand ratio increases, which can be attributed to the changing proportions of the electroactive $BuMg^+$ and $MgCl^+$ in the solutions.[106] Despite the difference in the exchange current density, the shapes of the Tafel and the Allen-Hickling plots were surprisingly similar for all solution compositions studied: the latter plots showed a linear dependence in a very narrow range of overpotential close to $\eta = 0$. From the slope of this curve, the transfer coefficients for the cathodic and the anodic reactions

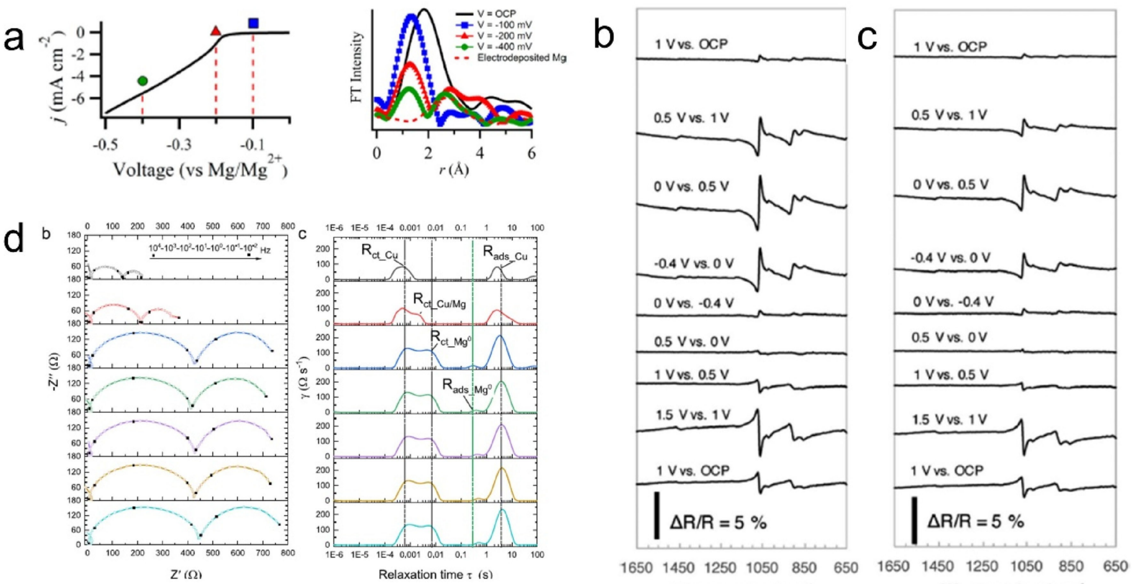

Figure 7. Exploitation of adsorption impacts on the electrified interface. a) Cathodic half-wave for deposition of Mg and highlighted potentials for the potentiostatic X-ray absorption experiments using 0.4 M EtMgCl-Et_2AlCl/THF. Fourier-transformed EXAFS spectra of the Mg K-edge at the Mg metal and electrolyte interface. Reproduced with permission from.[102] Copyright 2013 American Chemical Society; b, c) in situ FTIR spectra of a CV measurement using a Pt thin film electrode formed on the diamond window in 0.25 M EtMgCl–2Et_2AlCl in THF solution, between the OCV (1.32 V vs. Mg quasi-reference electrode) and −0.4 V vs. Mg quasi-reference electrode during the 1st CV cycle, and the 2nd cycle. Reproduced with permission from.[77] Copyright 2016 The Electrochemical Society; d) Operando EIS evolution and the corresponding analysis of DRT upon galvanostatic electrodeposition of Mg onto Cu at 0.5 mA cm^{-2} in 0.4 M $Mg(TFSI)_2$-0.1 M $Mg(BH_4)_2$/G2, Reproduced with permission from.[61] Copyright 2020 American Chemical Society.

were found to be around $\alpha_c = 0.5$ and $\alpha_a = 1.5$, which is strong evidence of two sequential one-electron transfers with the first electron transfer being the rate-determining step. The interplay relates to the same potential-dependent rate of the first-electron transfer (*i.e.* second in the dissolution process), and the potential-independent, preceding chemical reaction, *i.e.* diffusion of the Mg adatoms from the growth sites to the metallic sites.[3b]

The Mg^{2+}-blocking layers have been revealed in typical TFSI-based electrolytes (0.50 M $Mg(TFSI_2)$ in butyl methyl triglyme-BuMeG3 and 0.25 M EtMgCl-2Et2AlCl in **THF**) upon Mg plating.[77] Most peaks observed in the FTIR spectra for the 1st cathodic scan in the BuMeG3 electrolyte correspond to the $TFSI^-$ anion. The decomposed species remain as a passivation film to blocks both ion and electron transfer. This passivation layer was indirectly confirmed as MgF_2 by ex-situ X-ray photoelectron spectroscopy (XPS) measurement. MgF_2 has been considered electron-insulating and has high migration energy barrier for cation transport.[107] Although the migration energy of cations in both MgF_2 and CaF_2 is high, the inclusion of CaH_2 with much lower migration energy in the interphase of Ca metal anodes might be a key enabler for the reversible *plating/stripping*. However, in the electrolyte of 0.25 M EtMgCl–2Et_2AlCl in **THF**, the Pt working electrode was not passivated during the two times anodic and cathodic scans (Figure 7b, c) due to the suppressed decomposition of $TFSI^-$.

Apart from the complex adsorbates in Grignard-based or inorganic electrolytes, a relatively simple electrolyte of 0.4 M $MgTFSI_2$_0.1 M $Mg(BH_4)_2$_**G2** has been studied to demonstrate a critical adsorption step of Mg cation clusters onto the electrified interface for the reversible Mg *plating/stripping*.[61] A new impedance analysis method, *i.e.* distribution of relaxation time (DRT), was employed to deconvolute the evolution of impedance spectra on Cu electrode during Mg deposition. From the DRT analysis, they unveiled a new sluggish electrochemical process (10–0.01 Hz), which precede the charge-transfer process (10^4–10^2 Hz), in the impedance spectra during Mg electrodeposits (Figure 7d). This new electrochemical process is associated with the adsorption of active Mg species with BH_4^- onto new Mg electrodeposits. It is noted that understanding the dynamic interface characteristics of divalent metal anodes is essential to control its overall electrochemistry, which can be partially gained utilizing the impedance or XAS analysis. The adsorption step prior to the Mg was further confirmed by operando potentiostatic XAS measurement, which showed a clear sign of the pre-edge shift of the Mg K-edge in the BH_4^--containing electrolytes, while baseline electrolyte without BH_4^- anion kept unchanged upon the potential applied. This chemical difference corresponds to the adsorption of active cation species before the charge transfer reaction occurs.

For the reversible Mg *plating/stripping*, the adsorption process with Cl^- or BH_4^- species is found to be a key step for accelerating the charge-transfer kinetics.[108] The fully coordinated solvation structure of Mg^{2+} in the bulk electrolytes or the outer Helmholtz plane diffuses to the inner Helmholtz layer while retaining the strong coordinating species and expelling the weakly coordinating species. Afterward, the adsorbed active cation clusters undergo the following charge-transfer reactions

(Figure 6c). Depending on the electrochemical stability of anions involved in the active cation clusters adsorbed onto the electrified interface, the composition of interface layers and interface characteristics will significantly be regulated. Thus, it could be a feasible way of regulating the electrochemical double layer and charge-transfer kinetics for divalent metal *plating/stripping*.

3.4. Electrodeposition Morphology

Mg has been considered as a "non-dendrite" metal anode. It has been known that Mg anodes have attributed the low propensity for dendrite formation to small self-diffusion barriers and small Ehrlich-Schwoebel barriers for three-dimensional (3D) diffusion.[109] The faster surface diffusion of Mg adatoms along the Mg(0001) plane predicted through first-principles calculations is proposed to reduce dendritic growth, together with low diffusion barriers across steps and terraces. Self-diffusion coefficients, Ehrlich-Schwoebel barriers, and anisotropy resulting from the intrinsic crystal structure have emerged as some putative descriptors for comparing the dendrite-forming nature of different metal anode materials.[110] Based on the first-principles study, it was revealed that the free energy difference between crystals with different shapes is more significant for Mg than Li due to the stronger bonding between Mg atoms.[111] The electrochemical deposition of Mg is preferable to form high dimensional morphologies instead of 1D dendrite as in the case of Li.

It was found that the microstructure and chemistry of the Mg films, along with their overall cycling efficiency, showed a strong dependence on electrolyte chloride content (Figure 8).[78] The films formed using chloride-free TFSI that only has an 80% cycling efficiency showed much smaller grains and a more random texture. Electrochemically conditioned **MACC** and **MTPA** also led to smaller amounts of impurity being incorporated in the films than the case for TFSI electrolytes. The impurities tend to form discontinuous films orthogonal to the [0001] direction. This selective impurity accumulation directs Mg growth along non-[0001] directions in the TFSI electrolyte.

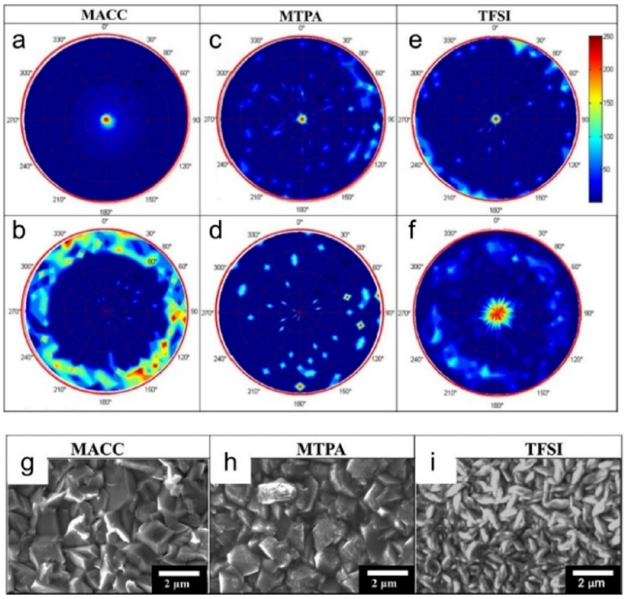

Figure 8. Dependence of morphology on electrolytes. (002) and (100) pole figures and SEM images of Mg layers deposited on Au (111) using (a, b, g) MACC, (c, d, h) MTPA, and (e, f, i) TFSI electrolytes respectively. Reproduced with permission from.[78] Copyright 2016 The Electrochemical Society.

In addition to impacts from electrolyte species, the applied current density has been revealed to exert a great impact on the morphology of Mg electrodeposits using Grignard-based electrolytes. Matsui[106] found the Mg deposit obtained at low current density showed (0001) preferred orientation, where the surface energy can be minimized during the slow deposition process. However, the Mg deposit obtained at high current density showed $(10\bar{1}0)$ preferred orientation formed by maximizing the crystal growth speed for a high deposition rate. Both deposits did not show any dendritic morphology. It should be noted that the Mg-ion transference number is typically low ($t^+ = 0.018$ for $[Mg_2(\boldsymbol{\mu}\text{-}\mathbf{Cl})_3 \cdot 6\mathbf{THF}]^+$, $t^+ = 0.130$ for **DCC**, $t^+ = 0.159$ for **APC**, $t^+ = 0.141$ for $Mg(TFSI)_2$/**G2**).[26a] At high current densities, the local supply or stability of Mg cation active species, with the aid of the adsorption agent of Cl^- or BH_4^-, could become insufficient or even depleted at the Sand time, which in turn drastically change the morphology of Mg electrodeposits.[112] In other words, one critical advantage of Mg anode (*i.e.* non-dendritic growth) has been rebutted by experimental observation of 3D growth character of Mg electrodeposits and consequent internal short-circuit of the cells in $MgTFSI_2$-based electrolytes.[112b,113] As such abnormal growth character of Mg may not be limited to the $MgTFSI_2$-based electrolytes, the rational design of separators or the use of solid-state electrolytes should be considered to realize the practical realization of rechargeable Mg batteries.

4. Summary and Future Considerations

The solution chemistry and interfacial electrochemistry of divalent electrolytes and metal anodes are substantially more complex than those of the monovalent counterpart, which presents a greater challenge in identifying and implementing practical battery chemistry based on divalent metals. Significant progress has been made in divalent electrolyte systems in the past years. The local interface environments, in which reversible divalent metal *plating/stripping* takes place are much more complex, including the dynamic equilibrium between electroactive divalent metal species and other supporting electrolyte species, which is well under-explored and presents great opportunities for scientific discovery.

There is still much yet to learn about the interplay between electrolyte agent adsorptions and the inner Helmholtz plane (the charge-transfer process), which could pave the way for artificial surface layers to enable reversible and stable divalent metal/electrolyte interface. The fundamental studies on the solvation structure/dynamic of electroactive species in relevant electrolyte solutions, the adsorption-deposition-dissolution mechanism on divalent metal anodes, and the insertion mechanism of electroactive cation species into high voltage cathodes will advance the fundamental understanding that will establish the scientific basis for the development of practical rechargeable divalent batteries.

Formulating the electrolyte solutions must be a key enabler to implement the multivalent metal batteries in practical applications. The non-passivating surface chemistry of divalent metal anodes will be a good subject for the non-destructive/time-resolved characterization to allow the active species on the electrified interface to be tracked. High-throughput theoretical investigation, *e.g.* machine learning, on the structural stability of the simulated host materials and diffusivity of divalent metal cations could advance the materials discovery on the premise that the electrolyte solutions with wide-potential stability are formulated in near future.

Acknowledgements

This work was supported as part of the Joint Center for Energy Storage Research (JCESR), an Energy Innovation Hub funded by the U.S. Department of Energy (DOE), Office of Science, Basic Energy Sciences. We're thankful to previous team members and collaborators who have worked on this collaborative research

Conflict of Interest

The authors declare no conflict of interest.

Keywords: divalent metal batteries · electrolytes · solution chemistry · interfaces · electrochemistry

[1] Y. Liang, H. Dong, D. Aurbach, Y. Yao, *Nat. Energy* **2020**, *5*, 646–656.

[2] a) A. M. Melemed, A. Khurram, B. M. Gallant, *Batteries & Supercaps* **2020**, *3*, 570–580; b) J. Muldoon, C. B. Bucur, T. Gregory, *Chem. Rev.* **2014**, *114*, 11683–11720; c) P. Canepa, G. Sai Gautam, D. C. Hannah, R. Malik, M. Liu, K. G. Gallagher, K. A. Persson, G. Ceder, *Chem. Rev.* **2017**, *117*, 4287–4341.

[3] a) J. Muldoon, C. B. Bucur, A. G. Oliver, T. Sugimoto, M. Matsui, H. S. Kim, G. D. Allred, J. Zajicek, Y. Kotani, *Energy Environ. Sci.* **2012**, *5*, 5941–5950; b) H. D. Yoo, I. Shterenberg, Y. Gofer, G. Gershinsky, N. Pour, D. Aurbach, *Energy Environ. Sci.* **2013**, *6*, 2265–2279; c) H. D. Yoo, J. R. Jokisaari, Y.-S. Yu, B. J. Kwon, L. Hu, S. Kim, S.-D. Han, M. Lopez, S. H. Lapidus, G. M. Nolis, B. J. Ingram, I. Bolotin, S. Ahmed, R. F. Klie, J. T. Vaughey, T. T. Fister, J. Cabana, *ACS Energy Lett.* **2019**, *4*, 1528–1534; d) J. L. Andrews, A. Mukherjee, H. D. Yoo, A. Parija, P. M. Marley, S. Fakra, D. Prendergast, J. Cabana, R. F. Klie, S. Banerjee, *Chem* **2018**, *4*, 564–585.

[4] a) M. Li, J. Lu, X. Ji, Y. Li, Y. Shao, Z. Chen, C. Zhong, K. Amine, *Nat. Rev. Mater.* **2020**, *5*, 276–294; b) J. Niu, Z. Zhang, D. Aurbach, *Adv. Energy Mater.* **2020**, *10*, 2000697.

[5] a) N. Amir, Y. Vestfrid, O. Chusid, Y. Gofer, D. Aurbach, *J. Power Sources* **2007**, *174*, 1234–1240; b) B. Park, J. L. Schaefer, *J. Electrochem. Soc.* **2020**, *167*, 070545; c) Y. Shao, N. N. Rajput, J. Hu, M. Hu, T. Liu, Z. Wei, M. Gu, X. Deng, S. Xu, K. S. Han, J. Wang, Z. Nie, G. Li, K. R. Zavadil, J. Xiao, C. Wang, W. A. Henderson, J.-G. Zhang, Y. Wang, K. T. Mueller, K. Persson, J. Liu, *Nano Energy* **2015**, *12*, 750–759; d) R. Deivanayagam, B. J. Ingram, R. Shahbazian-Yassar, *Energy Storage Mater.* **2019**, *21*, 136–153; e) R. Attias, M. Salama, B. Hirsch, Y. Goffer, D. Aurbach, *Joule* **2019**, *3*, 27–52.

[6] M. Mao, T. Gao, S. Hou, C. Wang, *Chem. Soc. Rev.* **2018**, *47*, 8804–8841.

[7] a) R. Mohtadi, O. Tutusaus, T. S. Arthur, Z. Zhao-Karger, M. Fichtner, *Joule* **2021**; b) P. Bonnick, J. Muldoon, *Adv. Funct. Mater.* **2020**, *30*, 1910510; c) M. E. Arroyo-de Dompablo, A. Ponrouch, P. Johansson, M. R. Palacín, *Chem. Rev.* **2020**, *120*, 6331–6357; d) Y. Tian, G. Zeng, A. Rutt, T. Shi, H. Kim, J. Wang, J. Koettgen, Y. Sun, B. Ouyang, T. Chen, Z. Lun, Z. Rong, K. Persson, G. Ceder, *Chem. Rev.* **2021**, *121*, 1623–1669.

[8] a) L. W. Gaddum, H. E. French, *J. Am. Chem. Soc.* **1927**, *49*, 1295–1299; b) W. V. Evans, F. H. Lee, *J. Am. Chem. Soc.* **1934**, *56*, 654–657.

[9] T. D. Gregory, *J. Electrochem. Soc.* **1990**, *137*, 775.

[10] C. Liebenow, Z. Yang, P. Lobitz, *Electrochem. Commun.* **2000**, *2*, 641–645.

[11] D. Aurbach, Z. Lu, A. Schechter, Y. Gofer, H. Gizbar, R. Turgeman, Y. Cohen, M. Moshkovich, E. Levi, *Nature* **2000**, *407*, 724–727.

[12] N. Pour, Y. Gofer, D. T. Major, D. Aurbach, *J. Am. Chem. Soc.* **2011**, *133*, 6270–6278.

[13] Y.-s. Guo, F. Zhang, J. Yang, F.-f. Wang, Y. NuLi, S.-i. Hirano, *Energy Environ. Sci.* **2012**, *5*, 9100–9106.

[14] H. S. Kim, T. S. Arthur, G. D. Allred, J. Zajicek, J. G. Newman, A. E. Rodnyansky, A. G. Oliver, W. C. Boggess, J. Muldoon, *Nat. Commun.* **2011**, *2*, 427.

[15] F.-f. Wang, Y.-s. Guo, J. Yang, Y. Nuli, S.-i. Hirano, *Chem. Commun.* **2012**, *48*, 10763–10765.

[16] C. Liao, B. Guo, D.-e. Jiang, R. Custelcean, S. M. Mahurin, X.-G. Sun, S. Dai, *J. Mater. Chem. A* **2014**, *2*, 581–584.

[17] K. Sato, G. Mori, T. Kiyosu, T. Yaji, K. Nakanishi, T. Ohta, K. Okamoto, Y. Orikasa, *Sci. Rep.* **2020**, *10*, 7362.

[18] a) R. E. Doe, R. Han, J. Hwang, A. J. Gmitter, I. Shterenberg, H. D. Yoo, N. Pour, D. Aurbach, *Chem. Commun.* **2014**, *50*, 243–245; b) K. A. See, Y.-M. Liu, Y. Ha, C. J. Barile, A. A. Gewirth, *ACS Appl. Mater. Interfaces* **2017**, *9*, 35729–35739; c) C. J. Barile, R. G. Nuzzo, A. A. Gewirth, *J. Phys. Chem. C* **2015**, *119*, 13524–13534.

[19] D. Lv, D. Tang, Y. Duan, M. L. Gordin, F. Dai, P. Zhu, J. Song, A. Manivannan, D. Wang, *J. Mater. Chem. A* **2014**, *2*, 15488–15494.

[20] O. Tutusaus, R. Mohtadi, T. S. Arthur, F. Mizuno, E. G. Nelson, Y. V. Sevryugina, *Angew. Chem. Int. Ed.* **2015**, *54*, 7900–7904; *Angew. Chem.* **2015**, *127*, 8011–8015.

[21] S. G. McArthur, L. Geng, J. Guo, V. Lavallo, *Inorg. Chem. Front.* **2015**, *2*, 1101–1104.

[22] S. G. McArthur, R. Jay, L. Geng, J. Guo, V. Lavallo, *Chem. Commun.* **2017**, *53*, 4453–4456.

[23] N. T. Hahn, T. J. Seguin, K.-C. Lau, C. Liao, B. J. Ingram, K. A. Persson, K. R. Zavadil, *J. Am. Chem. Soc.* **2018**, *140*, 11076–11084.

[24] a) H. Dong, O. Tutusaus, Y. Liang, Y. Zhang, Z. Lebens-Higgins, W. Yang, R. Mohtadi, Y. Yao, *Nat. Energy* **2020**, *5*, 1043–1050; b) H. Dong, Y. Liang, O. Tutusaus, R. Mohtadi, Y. Zhang, F. Hao, Y. Yao, *Joule* **2019**, *3*, 782–793.

[25] E. N. Keyzer, H. F. J. Glass, Z. Liu, P. M. Bayley, S. E. Dutton, C. P. Grey, D. S. Wright, *J. Am. Chem. Soc.* **2016**, *138*, 8682–8685.

[26] a) N. Sa, N. N. Rajput, H. Wang, B. Key, M. Ferrandon, V. Srinivasan, K. A. Persson, A. K. Burrell, J. T. Vaughey, *RSC Adv.* **2016**, *6*, 113663–113670; b) I. Shterenberg, M. Salama, H. D. Yoo, Y. Gofer, J.-B. Park, Y.-K. Sun, D. Aurbach, *J. Electrochem. Soc.* **2015**, *162*, A7118–A7128.

[27] D.-T. Nguyen, A. Y. S. Eng, M.-F. Ng, V. Kumar, Z. Sofer, A. D. Handoko, G. S. Subramanian, Z. W. Seh, *Cell Reports Physical Science* **2020**, *1*, 100265.

[28] R. Mohtadi, M. Matsui, T. S. Arthur, S.-J. Hwang, *Angew. Chem. Int. Ed.* **2012**, *51*, 9780–9783; *Angew. Chem.* **2012**, *124*, 9918–9921.

[29] a) Y. Shao, T. Liu, G. Li, M. Gu, Z. Nie, M. Engelhard, J. Xiao, D. Lv, C. Wang, J.-G. Zhang, J. Liu, *Sci. Rep.* **2013**, *3*, 3130; b) M. Salama, I. Shterenberg, L. J. W. Shimon, K. Keinan-Adamsky, M. Afri, Y. Gofer, D. Aurbach, *J. Phys. Chem. C* **2017**, *121*, 24909–24918.

[30] a) T. Watkins, A. Kumar, D. A. Buttry, *J. Am. Chem. Soc.* **2016**, *138*, 641–650; b) S. Su, Y. NuLi, N. Wang, D. Yusipu, J. Yang, J. Wang, *J. Electrochem. Soc.* **2016**, *163*, D682-D688; c) Y. Bi, S. He, C. Fan, J. Luo, B. Yuan, T. L. Liu, *J. Mater. Chem. A* **2020**, *8*, 12301–12305.

[31] N. N. Rajput, X. Qu, N. Sa, A. K. Burrell, K. A. Persson, *J. Am. Chem. Soc.* **2015**, *137*, 3411–3420.

[32] K. Xu, *Chem. Rev.* **2014**, *114*, 11503–11618.

[33] J. T. Herb, C. A. Nist-Lund, C. B. Arnold, *ACS Energy Lett.* **2016**, *1*, 1227–1232.

[34] Z. Zhao-Karger, M. E. Gil Bardaji, O. Fuhr, M. Fichtner, *J. Mater. Chem. A* **2017**, *5*, 10815–10820.

[35] A. Du, Z. Zhang, H. Qu, Z. Cui, L. Qiao, L. Wang, J. Chai, T. Lu, S. Dong, T. Dong, H. Xu, X. Zhou, G. Cui, *Energy Environ. Sci.* **2017**, *10*, 2616–2625.

[36] Z. Zhang, Z. Cui, L. Qiao, J. Guan, H. Xu, X. Wang, P. Hu, H. Du, S. Li, X. Zhou, S. Dong, Z. Liu, G. Cui, L. Chen, *Adv. Energy Mater.* **2017**, *7*, 1602055.

[37] T. Mandai, *ACS Appl. Mater. Interfaces* **2020**, *12*, 39135–39144.

[38] Z. Li, O. Fuhr, M. Fichtner, Z. Zhao-Karger, *Energy Environ. Sci.* **2019**, *12*, 3496–3501.

[39] A. Shyamsunder, L. E. Blanc, A. Assoud, L. F. Nazar, *ACS Energy Lett.* **2019**, *4*, 2271–2276.

[40] K. V. Nielson, J. Luo, T. L. Liu, *Batteries & Supercaps* **2020**, *3*, 766–772.

[41] J. Luo, Y. Bi, L. Zhang, X. Zhang, T. L. Liu, *Angew. Chem. Int. Ed.* **2019**, *58*, 6967–6971; *Angew. Chem.* **2019**, *131*, 7041–7045.

[42] C. B. Bucur, T. Gregory, A. G. Oliver, J. Muldoon, *J. Phys. Chem. Lett.* **2015**, *6*, 3578–3591.

[43] a) K.-C. Lau, T. J. Seguin, E. V. Carino, N. T. Hahn, J. G. Connell, B. J. Ingram, K. A. Persson, K. R. Zavadil, C. Liao, *J. Electrochem. Soc.* **2019**, *166*, A1510–A1519; b) J. H. Ha, B. Lee, M. Lee, T. Yim, S. H. Oh, *Chem. Commun.* **2020**, *56*, 14163–14166.

[44] K. V. Nielson, T. L. Liu, *Angew. Chem. Int. Ed.* **2020**, *59*, 3368–3370; *Angew. Chem.* **2020**, *132*, 3392–3394.

[45] N. N. Rajput, T. J. Seguin, B. M. Wood, X. Qu, K. A. Persson, *Top. Curr. Chem.* **2018**, *376*, 19.

[46] a) A. Baskin, D. Prendergast, *J. Phys. Chem. C* **2016**, *120*, 3583–3594; b) J. Z. Hu, N. R. Jaegers, Y. Chen, K. S. Han, H. Wang, V. Murugesan, K. T. Mueller, *ACS Appl. Mater. Interfaces* **2019**, *11*, 38689–38696.

[47] A. Baskin, D. Prendergast, *J. Phys. Chem. Lett.* **2019**, *10*, 4920–4928.

[48] R. E. Doe, G. H. Lane, R. E. Jilek, J. Hwang, PELLION TECHNOLOGIES, INC., Cambridge, MA (United States), **2016**, p. Medium: ED.

[49] K. Shimokawa, H. Matsumoto, T. Ichitsubo, *J. Phys. Chem. Lett.* **2018**, *9*, 4732–4737.

[50] Y. Cheng, R. M. Stolley, K. S. Han, Y. Shao, B. W. Arey, N. M. Washton, K. T. Mueller, M. L. Helm, V. L. Sprenkle, J. Liu, G. Li, *Phys. Chem. Chem. Phys.* **2015**, *17*, 13307–13314.

[51] a) Z. Zhao-Karger, J. E. Mueller, X. Zhao, O. Fuhr, T. Jacob, M. Fichtner, *RSC Adv.* **2014**, *4*, 26924–26927; b) Z. Zhao-Karger, X. Zhao, D. Wang, T. Diemant, R. J. Behm, M. Fichtner, *Adv. Energy Mater.* **2015**, *5*, 1401155.

[52] T. Liu, Y. Shao, G. Li, M. Gu, J. Hu, S. Xu, Z. Nie, X. Chen, C. Wang, J. Liu, *J. Mater. Chem. A* **2014**, *2*, 3430–3438.

[53] C. Liao, N. Sa, B. Key, A. K. Burrell, L. Cheng, L. A. Curtiss, J. T. Vaughey, J.-J. Woo, L. Hu, B. Pan, Z. Zhang, *J. Mater. Chem. A* **2015**, *3*, 6082–6087.

[54] T. Gao, M. Noked, A. J. Pearse, E. Gillette, X. Fan, Y. Zhu, C. Luo, L. Suo, M. A. Schroeder, K. Xu, S. B. Lee, G. W. Rubloff, C. Wang, *J. Am. Chem. Soc.* **2015**, *137*, 12388–12393.

[55] H. Fan, Z. Zheng, L. Zhao, W. Li, J. Wang, M. Dai, Y. Zhao, J. Xiao, G. Wang, X. Ding, H. Xiao, J. Li, Y. Wu, Y. Zhang, *Adv. Funct. Mater.* **2020**, *30*, 1909370.

[56] D. Huang, S. Tan, M. Li, D. Wang, C. Han, Q. An, L. Mai, *ACS Appl. Mater. Interfaces* **2020**, *12*, 17474–17480.

[57] J. Z. Hu, N. N. Rajput, C. Wan, Y. Shao, X. Deng, N. R. Jaegers, M. Hu, Y. Chen, Y. Shin, J. Monk, Z. Chen, Z. Qin, K. T. Mueller, J. Liu, K. A. Persson, *Nano Energy* **2018**, *46*, 436–446.

[58] Z. Zhao-Karger, X. Zhao, O. Fuhr, M. Fichtner, *RSC Adv.* **2013**, *3*, 16330–16335.

[59] N. T. Hahn, J. Self, T. J. Seguin, D. M. Driscoll, M. A. Rodriguez, M. Balasubramanian, K. A. Persson, K. R. Zavadil, *J. Mater. Chem. A* **2020**, *8*, 7235–7244.

[60] K. Ta, R. Zhang, M. Shin, R. T. Rooney, E. K. Neumann, A. A. Gewirth, *ACS Appl. Mater. Interfaces* **2019**, *11*, 21536–21542.

[61] H. Wang, X. Feng, Y. Chen, Y.-S. Liu, K. S. Han, M. Zhou, M. H. Engelhard, V. Murugesan, R. S. Assary, T. L. Liu, W. Henderson, Z. Nie, M. Gu, J. Xiao, C. Wang, K. Persson, D. Mei, J.-G. Zhang, K. T. Mueller, J. Guo, K. Zavadil, Y. Shao, J. Liu, *ACS Energy Lett.* **2020**, *5*, 200–206.

[62] H. Xu, Z. Zhang, J. Li, L. Qiao, C. Lu, K. Tang, S. Dong, J. Ma, Y. Liu, X. Zhou, G. Cui, *ACS Appl. Mater. Interfaces* **2018**, *10*, 23757–23765.

[63] Y. Jie, Y. Tan, L. Li, Y. Han, S. Xu, Z. Zhao, R. Cao, X. Ren, F. Huang, Z. Lei, G. Tao, G. Zhang, S. Jiao, *Angew. Chem. Int. Ed.* **2020**, *59*, 12689–12693; *Angew. Chem.* **2020**, *132*, 12789–12793.

[64] N. T. Hahn, J. Self, K. S. Han, V. Murugesan, K. T. Mueller, K. A. Persson, K. R. Zavadil, *J. Phys. Chem. B* **2021**, *125*, 3644–3652.

[65] H. D. Yoo, S.-D. Han, I. L. Bolotin, G. M. Nolis, R. D. Bayliss, A. K. Burrell, J. T. Vaughey, J. Cabana, *Langmuir* **2017**, *33*, 9398–9406.

[66] S.-Y. Ha, Y.-W. Lee, S. W. Woo, B. Koo, J.-S. Kim, J. Cho, K. T. Lee, N.-S. Choi, *ACS Appl. Mater. Interfaces* **2014**, *6*, 4063–4073.

[67] M. Salama, I. Shterenberg, H. Gizbar, N. N. Eliaz, M. Kosa, K. Keinan-Adamsky, M. Afri, L. J. W. Shimon, H. E. Gottlieb, D. T. Major, Y. Gofer, D. Aurbach, *J. Phys. Chem. C* **2016**, *120*, 19586–19594.

[68] Y. Chen, N. R. Jaegers, K. S. Han, H. Wang, R. P. Young, G. Agarwal, A. S. Lipton, R. S. Assary, N. M. Washton, J. Z. Hu, K. T. Mueller, V. Murugesan, *J. Phys. Chem. C* **2020**, *124*, 4999–5008.

[69] S. Fan, G. M. Asselin, B. Pan, H. Wang, Y. Ren, J. T. Vaughey, N. Sa, *ACS Appl. Mater. Interfaces* **2020**, *12*, 10252–10260.

[70] M. Hattori, K. Yamamoto, M. Matsui, K. Nakanishi, T. Mandai, A. Choudhary, Y. Tateyama, K. Sodeyama, T. Uchiyama, Y. Orikasa, Y. Tamenori, T. Takeguchi, K. Kanamura, Y. Uchimoto, *J. Phys. Chem. C* **2018**, *122*, 25204–25210.

[71] F. Tuerxun, K. Yamamoto, M. Hattori, T. Mandai, K. Nakanishi, A. Choudhary, Y. Tateyama, K. Sodeyama, A. Nakao, T. Uchiyama, M. Matsui, K. Tsuruta, Y. Tamenori, K. Kanamura, Y. Uchimoto, *ACS Appl. Mater. Interfaces* **2020**, *12*, 25775–25785.

[72] a) Y. Yu, A. Baskin, C. Valero-Vidal, N. T. Hahn, Q. Liu, K. R. Zavadil, B. W. Eichhorn, D. Prendergast, E. J. Crumlin, *Chem. Mater.* **2017**, *29*, 8504–8512; b) R. Jay, A. W. Tomich, J. Zhang, Y. Zhao, A. De Gorostiza, V. Lavallo, J. Guo, *ACS Appl. Mater. Interfaces* **2019**, *11*, 11414–11420; c) A. Kopač Lautar, J. Bitenc, T. Rejec, R. Dominko, J.-S. Filhol, M.-L. Doublet, *J. Am. Chem. Soc.* **2020**, *142*, 5146–5153.

[73] J. G. Connell, M. Zorko, G. Agarwal, M. Yang, C. Liao, R. S. Assary, D. Strmcnik, N. M. Markovic, *ACS Appl. Mater. Interfaces* **2020**, *12*, 36137–36147.

[74] N. T. Hahn, D. M. Driscoll, Z. Yu, G. E. Sterbinsky, L. Cheng, M. Balasubramanian, K. R. Zavadil, *ACS Appl. Mater. Interfaces* **2020**, *3*, 8437–8447.

[75] J. G. Connell, B. Genorio, P. P. Lopes, D. Strmcnik, V. R. Stamenkovic, N. M. Markovic, *Chem. Mater.* **2016**, *28*, 8268–8277.

[76] T. Yim, S.-G. Woo, S.-H. Lim, J.-Y. Yoo, W. Cho, M.-S. Park, Y.-K. Han, Y.-J. Kim, J. Yu, *ACS Sustainable Chem. Eng.* **2017**, *5*, 5733–5739.

[77] H. Kuwata, M. Matsui, N. Imanishi, *J. Electrochem. Soc.* **2017**, *164*, A3229-A3236.

[78] M. N. Bachhav, N. T. Hahn, K. R. Zavadil, E. G. Nelson, A. J. Crowe, B. M. Bartlett, P.-W. Chu, V. J. Araullo-Peters, E. A. Marquis, *J. Electrochem. Soc.* **2016**, *163*, D645-D650.

[79] a) R. J. Staniewicz, *J. Electrochem. Soc.* **1980**, *127*, 782; b) E. Peled, R. Tulman, A. Meitav, *J. Power Sources* **1983**, *10*, 125–135; c) A. Meitav, E. Peled, *Electrochim. Acta* **1988**, *33*, 1111–1121.

[80] A. Ponrouch, C. Frontera, F. Bardé, M. R. Palacín, *Nat. Mater.* **2016**, *15*, 169–172.

[81] D. Wang, X. Gao, Y. Chen, L. Jin, C. Kuss, P. G. Bruce, *Nat. Mater.* **2018**, *17*, 16–20.

[82] S.-B. Son, T. Gao, S. P. Harvey, K. X. Steirer, A. Stokes, A. Norman, C. Wang, A. Cresce, K. Xu, C. Ban, *Nat. Chem.* **2018**, *10*, 532–539.

[83] X. Li, T. Gao, F. Han, Z. Ma, X. Fan, S. Hou, N. Eidson, W. Li, C. Wang, *Adv. Energy Mater.* **2018**, *8*, 1701728.

[84] B. Li, R. Masse, C. Liu, Y. Hu, W. Li, G. Zhang, G. Cao, *Energy Storage Mater.* **2019**, *22*, 96–104.

[85] R. Lv, X. Guan, J. Zhang, Y. Xia, J. Luo, *Natl. Sci. Rev.* **2019**, *7*, 333–341.

[86] K. Tang, A. Du, S. Dong, Z. Cui, X. Liu, C. Lu, J. Zhao, X. Zhou, G. Cui, *Adv. Mater.* **2020**, *32*, 1904987.

[87] J. Zhang, X. Guan, R. Lv, D. Wang, P. Liu, J. Luo, *Energy Storage Mater.* **2020**, *26*, 408–413.

[88] Z. Liang, C. Ban, *Angew. Chem. Int. Ed.* **2021**, n/a.

[89] K. Ta, K. A. See, A. A. Gewirth, *J. Phys. Chem. C* **2018**, *122*, 13790–13796.

[90] C. J. Barile, E. C. Barile, K. R. Zavadil, R. G. Nuzzo, A. A. Gewirth, *J. Phys. Chem. C* **2014**, *118*, 27623–27630.

[91] P. Canepa, S. Jayaraman, L. Cheng, N. N. Rajput, W. D. Richards, G. S. Gautam, L. A. Curtiss, K. A. Persson, G. Ceder, *Energy Environ. Sci.* **2015**, *8*, 3718–3730.

[92] K. A. See, K. W. Chapman, L. Zhu, K. M. Wiaderek, O. J. Borkiewicz, C. J. Barile, P. J. Chupas, A. A. Gewirth, *J. Am. Chem. Soc.* **2016**, *138*, 328–337.

[93] J. H. Ha, B. Adams, J.-H. Cho, V. Duffort, J. H. Kim, K. Y. Chung, B. W. Cho, L. F. Nazar, S. H. Oh, *J. Mater. Chem. A* **2016**, *4*, 7160–7164.

[94] J. Luo, S. He, T. L. Liu, *ACS Energy Lett.* **2017**, *2*, 1197–1202.

[95] G. Bieker, M. Salama, M. Kolek, Y. Gofer, P. Bieker, D. Aurbach, M. Winter, *ACS Appl. Mater. Interfaces* **2019**, *11*, 24057–24066.

[96] D. Aurbach, A. Schechter, M. Moshkovich, Y. Cohen, *J. Electrochem. Soc.* **2001**, *148*, A1004.

[97] D. Aurbach, R. Turgeman, O. Chusid, Y. Gofer, *Electrochem. Commun.* **2001**, *3*, 252–261.

[98] J. L. Esbenshade, C. J. Barile, T. T. Fister, K. L. Bassett, P. Fenter, R. G. Nuzzo, A. A. Gewirth, *J. Phys. Chem. C* **2015**, *119*, 23366–23372.
[99] T. S. Arthur, P.-A. Glans, M. Matsui, R. Zhang, B. Ma, J. Guo, *Electrochem. Commun.* **2012**, *24*, 43–46.
[100] Y. Nakayama, Y. Kudo, H. Oki, K. Yamamoto, Y. Kitajima, K. Noda, *J. Electrochem. Soc.* **2008**, *155*, A754.
[101] Y. Ye, C. H. Wu, L. Zhang, Y.-S. Liu, P.-A. Glans-Suzuki, J. Guo, *J. Electron Spectrosc. Relat. Phenom.* **2017**, *221*, 2–9.
[102] A. Benmayza, M. Ramanathan, T. S. Arthur, M. Matsui, F. Mizuno, J. Guo, P.-A. Glans, J. Prakash, *J. Phys. Chem. C* **2013**, *117*, 26881–26888.
[103] L. C. Kao, X. Feng, Y. Ha, F. Yang, Y.-S. Liu, N. T. Hahn, J. MacDougall, W. Chao, W. Yang, K. R. Zavadil, J. Guo, *Surf. Sci.* **2020**, *702*, 121720.
[104] P. Canepa, G. S. Gautam, R. Malik, S. Jayaraman, Z. Rong, K. R. Zavadil, K. Persson, G. Ceder, *Chem. Mater.* **2015**, *27*, 3317–3325.
[105] Y. Viestfrid, M. D. Levi, Y. Gofer, D. Aurbach, *J. Electroanal. Chem.* **2005**, *576*, 183–195.
[106] M. Matsui, *J. Power Sources* **2011**, *196*, 7048–7055.
[107] a) Z. Yi, R. Jia, *J. Phys. Condens. Matter* **2012**, *24*, 085602; b) T. Chen, G. Sai Gautam, P. Canepa, *Chem. Mater.* **2019**, *31*, 8087–8099; c) J. Forero-Saboya, C. Davoisne, R. Dedryvère, I. Yousef, P. Canepa, A. Ponrouch, *Energy Environ. Sci.* **2020**, *13*, 3423–3431.
[108] C. Yan, H.-R. Li, X. Chen, X.-Q. Zhang, X.-B. Cheng, R. Xu, J.-Q. Huang, Q. Zhang, *J. Am. Chem. Soc.* **2019**, *141*, 9422–9429.
[109] a) M. Jäckle, K. Helmbrecht, M. Smits, D. Stottmeister, A. Groß, *Energy Environ. Sci.* **2018**, *11*, 3400–3407; b) J. N. Chazalviel, *Phys. Rev. A* **1990**, *42*, 7355–7367.
[110] H. Wang, M. Matsui, H. Kuwata, H. Sonoki, Y. Matsuda, X. Shang, Y. Takeda, O. Yamamoto, N. Imanishi, *Nat. Commun.* **2017**, *8*, 15106.
[111] C. Ling, D. Banerjee, M. Matsui, *Electrochim. Acta* **2012**, *76*, 270–274.
[112] a) R. Davidson, A. Verma, D. Santos, F. Hao, C. D. Fincher, D. Zhao, V. Attari, P. Schofield, J. Van Buskirk, A. Fraticelli-Cartagena, T. E. G. Alivio, R. Arroyave, K. Xie, M. Pharr, P. P. Mukherjee, S. Banerjee, *Mater. Horiz.* **2020**, *7*, 843–854; b) J. Eaves-Rathert, K. Moyer, M. Zohair, C. L. Pint, *Joule* **2020**, *4*, 1324–1336.
[113] M. S. Ding, T. Diemant, R. J. Behm, S. Passerini, G. A. Giffin, *J. Electrochem. Soc.* **2018**, *165*, A1983–A1990.

Manuscript received: April 13, 2021
Revised manuscript received: May 28, 2021
Accepted manuscript online: June 4, 2021

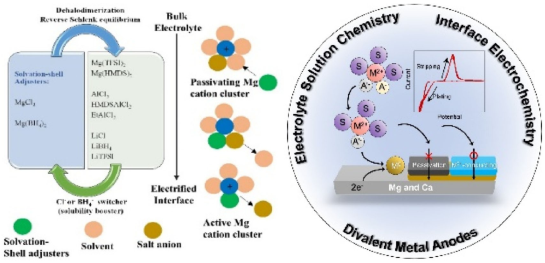

Elucidation of the interplay between electrolyte structure and interface electrochemistry of divalent metal anodes is essential to realize high-volumetric-energy-density rechargeable divalent metal batteries. This minireview discusses the design of electrolytes, from classical to advanced, that involves different solvation structures related to anion species and their interplays with interfacial dynamics and electrochemistry of divalent metal anodes.

Dr. H. Wang, Dr. J. Ryu, Dr. Y. Shao, Dr. V. Murugesan, Prof. Dr. K. Persson, Dr. K. Zavadil, Dr. K. T. Mueller, Dr. J. Liu*

1 – 18

Advancing Electrolyte Solution Chemistry and Interfacial Electrochemistry of Divalent Metal Batteries